The Pennsylvania State University
The Graduate School

INVESTIGATING MID-LATITUDE ATMOSPHERIC VARIABILITY DUE TO ARCTIC SEA ICE LOSS USING SELF-ORGANIZING MAPS

A Thesis in
Meteorology and Atmospheric Science
by
Samantha Staskiewicz

Submitted in Partial Fulfillment
of the Requirements
for the Degree of

Master of Science

August 2021

The thesis of Samantha Staskiewicz was reviewed and approved by the following:

Melissa Gervais
Assistant Professor of Meteorology and Atmospheric Science
Thesis Advisor

Chris E. Forest
Professor of Climate Dynamics

Colin Zarzycki
Assistant Professor of Meteorology and Climate Dynamics

David J. Stensrud
Professor of Meteorology
Head of the Department of Meteorology and Atmospheric Science

Abstract

Arctic sea ice is declining rapidly as greenhouse gas levels and global temperatures continue to rise due to human activity. Although a robust response of the mean atmospheric circulation to sea ice loss is well established, the impact of future Arctic sea ice loss on atmospheric variability remains an open question. In this study, we analyze results from two fully coupled, "high top" Whole Atmosphere Community Climate Model (WACCM4) simulations, one with 1980-1999 seasonally varying sea ice conditions and the other with sea ice nudged to projected RCP 8.5 values over the period of 2080-2099. This model setup allows us to identify changes in atmospheric conditions directly caused by sea ice loss. To characterize atmospheric variability, we use an artificial neural network method called self organizing maps (SOMs) applied to daily DJF data over North America. The SOM method identifies the dominant patterns of atmospheric variability and how often they occur in the two simulations, allowing us to quantify the impact of sea ice loss on atmospheric circulation. Additionally, we composite days associated with each SOM node for additional variables to provide an understanding of the physical processes responsible for changes in variability between these simulations. We find the most significant responses to sea ice loss to occur in the form of modified cold air outbreaks where patterns of cold anomalies over North America become less cold but more frequent. Furthermore, we identify continental warm anomalies to become anomalously cold with sea ice loss, resulting from a contraction of the Aleutian Low which prevents warm, maritime air from reaching the continent. We also find patterns with increased Aleutian Lows to become more frequent overall with sea ice loss. This unique methodology allows us to gain better insight into how weather patterns over North America may change as a result of future Arctic sea ice loss.

Table of Contents

List of Figures

Acknowledgments

I would like to sincerely thank my advisor, Dr. Melissa Gervais, for her mentorship and guidance throughout my time as her research student. She taught me a great deal about being a dedicated researcher and about climate science as a field of study.

I would also like to thank the Gervais Research Group (Dr. Kevin Bowley, Qinxue "Sharon" Gu, and Grant LaChat) for their constant feedback on the progress of this project. Having a supportive team and multiple perspectives is always helpful and eye-opening!

This project would not have been possible without the model simulations from our collaborators, Dr. Lantao Sun and Dr. Clara Deser. Thank you for sharing your data with us and for making this project come to life.

Lastly, thank you to the entire Penn State Department of Meteorology and Atmospheric Science. My time at Penn State was invaluable and I will miss everyone in Happy Valley.

Chapter 1 Introduction

Sea ice is rapidly declining as increasing anthropogenic greenhouse gas emissions cause global temperatures to rise. The Arctic in particular is expected to be close to ice-free by 2030, and the probability of an ice-free Arctic in the summer is projected to increase as the magnitude of global warming approaches 2° (Wang and Overland, 2012; Jahn, 2018). Arctic sea ice plays a key role in Arctic ecosystems, as many polar species rely on organic compounds on the surface of the ice for food and brine rejection from sea ice into the ocean for ideal living conditions (Arrigo et al., 2014). The albedo of sea ice is also important for the Earth's radiative budget (Perovich and Polashenski, 2012).

A robust impact of Arctic sea ice loss is Arctic Amplification (AA), a phenomenon where the Arctic is warming faster than the global mean (Alexeev et al., 2012). Arctic sea ice loss can produce AA through the reduction in sea ice albedo, which causes the ocean to absorb more incoming solar radiation, leading to local warming (Stroeve et al., 2012; Dai and Deng, 2021). Additional mechanisms important for producing AA include lapse rate, water vapor, and cloud feedbacks (Pithan and Mauritsen, 2014). The AA signal can be seen in modeling studies with prescribed sea ice loss (Pithan and Mauritsen, 2014; Holland and Bitz, 2003; Stroeve et al., 2012; Wang and Overland, 2012; Barnes and Screen, 2015), as well as in observations (Serreze et al., 2000; Serreze and Francis, 2006; Serreze et al., 2009; Screen and Simmonds, 2010; Cohen et al., 2014). The increased atmospheric temperatures associated with AA are largest near the surface and decrease in magnitude at higher altitudes (Serreze et al., 2009; Screen, 2014; Meleshko et al., 2016; Kumar et al., 2010). This is also reflected in the mean atmospheric circulation where, for example, column integrated warming results in higher geopotential heights at 500hPa over the Arctic.

Although climate models are in broad agreement in terms of the existence of AA, the projections of the magnitude of AA can vary between models (Holland and

Bitz, 2003). These differences could result from differences in the model employed, magnitude or pattern of sea ice forcing, method used to impose the forcing (e.g. different nudging methods in fully coupled simulations), model's background SST and land surface, atmosphere-ocean coupling, and atmospheric variability (Smith et al., 2019). For example, Deser et al. (2015) identified the importance of coupling in order to accurately represent the mid-latitude response to AA by showing that coupled simulations produced circulation responses that were extended to lower latitudes and higher altitudes, thus more consistent with the observed AA. To address model differences, the World Climate Research Programme has developed the Polar Amplification Model Inter-comparison Project (PAMIP), an initiative with collaborators from all over the world that seeks to understand how differences in model regimes impact AA and surface temperature changes in the Antarctic (Smith et al., 2019). PAMIP creates a set of coordinated experiments with the same protocol so that different models can be directly compared. The main goals of PAMIP are to understand how sea ice and sea surface temperature (SST) individually contribute to polar amplification and how the global climate system responds to polar amplification (Smith et al., 2019).

In addition to the thermodynamic impacts of sea ice loss, many studies have explored its mean impact on atmospheric circulation in the mid-latitudes. Given the change in North-South temperature gradient associated with AA, it is expected that sea ice loss will result in a equatorward shift of upper level winds in the mid-latitudes due to thermal wind balance. This is borne out in modeling studies where there is broad agreement of an equatorward shift due to sea ice loss both in studies with prescribed SST and sea ice (Ronalds et al., 2020; Sun et al., 2015; Blackport and Kushner, 2017, 2018) and fully coupled studies with nudged sea ice (Screen et al., 2018; Deser et al., 2015). This is an important factor when considering the full impact of greenhouse gas emissions on the midlatitude jets, because where tropical heating tends to force a poleward shift of the jets, sea ice decline produces an equatorward shift in the midlatitude jets (Deser et al., 2015; Oudar et al., 2017; Blackport and Kushner, 2017). In addition to its impact on the midlatitude jets, several studies have also shown that sea ice loss can result in a deepened Aleutian Low over the Pacific (Blackport and Kushner, 2018; Screen et al., 2018).

Screen (2017) found the atmospheric response to sea ice loss to be different depending on the region of sea ice loss, and that the responses were non-additive. Of particular relevance to the circulation over North America, Screen (2017), Honda et al. (2009), and Williams et al. (2021) all found that sea ice loss in the Sea of Okhotsk results in a Rossby

wave propagating across the Pacific and over North America.

Studies based on observations (Overland et al., 2011; Hopsch et al., 2012; Rinke et al., 2013) and modelling (Alexander et al., 2004; Deser et al., 2004; Magnusdottir et al., 2004; Pedersen et al., 2016) have shown a negative NAO-AO like patterns as a result of sea ice loss. Several studies have found changes in vertical wave propagation in the stratospheric response of Arctic sea ice to have an impact on the mid-latitudes in the form of a negative NAO/AO (Jaiser et al., 2013; Nakamura et al., 2015; Sun et al., 2015). This could cause a weakening of the polar vortex in response to changes in vertical wave propagation in the Arctic (Matsuno, 1971). Pedersen et al. (2016) further found the centers of action of the NAO response to sea ice loss to shift depending on whether sea ice is reduced in the Pacific vs. Atlantic sectors of the Arctic.

Francis and Vavrus (2012) used reanalysis data to investigate atmospheric variability due to Arctic sea ice loss and found increased zonal winds, slower propagation of Rossby waves, and meridional elongation of waves, resulting in an increased frequency of blocking patterns over North America. However, Barnes and Polvani (2013) did not find any significant increases in wave amplitude resulting from Arctic sea ice loss over the historical period, and argued findings from Francis and Vavrus (2012) to be sensitive to the specifics of the methodology. Although these studies are examining sea ice loss over the historical period, unlike ours which looks at a much larger sea ice loss in the future, they are illustrative of the importance of methodology in identifying changes in atmospheric variability.

Cold air outbreaks (CAOs) are an impactful winter phenomenon over North America, and changes in CAOs have been attributed to Arctic sea ice decline. CAOs are generally defined as having persistent conditions of anomalously cold air, which may be classified as having temperatures of at least two standard deviations below the climatological average for at least two days (Vavrus et al., 2006).

The dominant mechanisms leading to CAOs include northerly cold air advection bringing cold polar air to the continent and local adiabatic cooling (Walsh et al., 2001). Walsh et al. (2001) also found negative NAO/AO signals to often be present at the time of CAOs. To investigate the variability of CAOs in response to Arctic sea ice loss, Screen (2014) used twenty-first century model simulations to analyze how atmospheric variance changed over time. When including the mean state in the analysis, Screen (2014) found decreases in wintertime atmospheric temperature variability over the mid-latitudes, specifically in the form of fewer and less severe cold extremes and a slight increase in days with warm conditions. However, Ayarzagüena and Screen (2016) considered

the changing climatological mean temperature with climate change, and used different temperature thresholds to accurately represent the mean state with future conditions. When comparing a set of simulations with different sea ice conditions, Ayarzagüena and Screen (2016) and Screen (2014) found that the cold extremes were less severe, but Ayarzagüena and Screen (2016) found no difference in frequency of occurrence of cold extremes. These two studies show that when different methodologies were considered, the interpretation of the variability changed. Choosing constant definitions of climate extremes can be useful if the value of the variable has physical implications, for example, temperatures below freezing having implications for agriculture. However, choosing a changing definition of the mean state with different forcings allows for the impact of sea ice loss on variability to be disentangled from the mean response. Since we are interested in understanding the role of sea ice on atmospheric variability in this study, we will choose a definition with respect to a changing background climate state.

Further studies including Mori et al. (2014) have also found mid-latitude cold extremes to be sensitive to the region of sea ice loss, specifically that sea ice loss in the Barents-Kara sea leads to an increased probability of significant cold anomalies over Eurasia. There is a wide range of evidence supporting this "Warm Arctic, Cold Continent" phenomenon, both in terms of the impact of overall Arctic sea ice loss, and that in smaller regional seas (Overland et al., 2011; Cohen et al., 2014; Chen and Luo, 2017; Sun et al., 2016; Mori et al., 2014; Inoue et al., 2012)

The goal of our study is to understand the impact of Arctic sea ice loss on daily atmospheric variability over North America. Understanding the day-to-day variability of the atmosphere can provide insight into the societal impacts of sea ice loss. We use data representing a future climate to better understand how atmospheric variability will change with the large sea ice loss expected in the future rather than how sea ice loss has caused changes in variability in the past. Changes in daily weather patterns may occur in addition to mean changes in atmospheric circulation, with potentially different magnitudes, impacts, and mechanisms responsible. We remove the seasonal cycle in order to isolate the impact of sea ice loss on atmospheric variability from the mean. Self-organizing maps (SOMs) are used to identify archetypes of daily variability in two simulations; one with historical sea ice conditions, and one with futuristic sea ice conditions. Differences in atmospheric variability are then established by quantifying how these archetypes differ in frequency and pattern between simulations. This provides a nuanced understanding of how daily weather patterns over North America may change as a result of Arctic sea ice loss.

In Chapter 2, we will describe the SOM algorithm and our methods for analyzing variability. In Chapter 3 we look at the mean impact of sea ice loss and examine the impact of Arctic sea ice loss on atmospheric variability. Chapter 4 will conclude our study and outline the goals of our future work.

Chapter 2
Data and Methods

2.1 Model Simulations

To investigate the contribution of sea ice loss to atmospheric variability, we employed a set of two Community Earth System Model (CESM) (Hurrell et al., 2013) simulations with constrained sea ice. The model setup utilizes the Whole Atmosphere Community Climate Model (WACCM4), the Parallel Ocean Program Version 2 (POP2), Community Land Model Version 4 (CLM4), and the Los Alamos Sea Ice Model (CICE4) component models. The atmosphere and land components both have horizontal resolutions of $1.9° \times 2.5°$, and the ocean and sea ice components have roughly $1°$ resolutions. The Whole Atmosphere Community Climate Model (WACCM4) is a high-top model with 66 vertical pressure levels reaching approximately 140 km or 5.96 x 10^{-6} hPa. The model also includes a sophisticated stratospheric chemistry package which provides more realistic conditions in the upper-atmosphere. The added vertical resolution and extension to higher heights leads to a better representation of the stratosphere. This is important for studying the impact of sea ice loss as troposphere-stratosphere interactions are known to be an important mechanism through which sea ice loss impacts the atmosphere. The CICE4 model includes a thermodynamic component that calculates growth rates of snow and ice, an ice dynamics component that utilizes realistic ice physics based on ice mass and velocity, a thickness parameterization that quantifies ice strain and thickness, and a transport model that simulates ice advection (Hunke et al., 2015).

The two experiments are fully-coupled with radiative forcing held constant at the year 2000. The control simulation (CNTRL) is nudged to 1980-1999 seasonally varying sea ice conditions and the experiment simulation (EXP) is nudged to projected RCP 8.5 values of the period of 2080-2099 taken from a CESM-WACCM historical run and a CESM-WACCM RCP 8.5 simulation respectively. The nudging method found in Deser

et al. (2015) utilizes both upward and downward long wave radiative fluxes (LRF) in each grid cell of the sea ice model to force the sea ice to mimic historical and projected sea ice conditions. The magnitude of the LRF varies by month, but does not vary spatially, and is applied only to the sea ice model where there is sea ice. The magnitude of the downward LRF is larger for months of greater ice thickness and coverage. Although energy is not conserved using this method, water is conserved between the sea ice and ocean model components. The experiments are both 300 years in duration, but we disregard the first 100 years for spin-up time and retain only the last 200 years for the analysis.

One advantage of this coupled model configuration is that sea surface temperature (SSTs) are free to vary. This allows for more realistic sea surface temperatures that are free to increase as the sea ice edge retreats and maintains dynamic atmosphere-ocean variability, which has been shown to be important for generating a more realistic response to sea ice loss that extend to lower latitudes and higher altitudes (Deser et al., 2015). Although the SSTs will differ between the simulations, they are still a direct bi-product of changes in sea ice as this is the only difference between the two model set-ups.

These simulations result in differences in sea ice cover that vary monthly. Figure 2.1a shows the monthly mean sea ice extent for each simulation, defined as the total area of grid boxes having at least 15% sea ice concentration. Sea ice loss is at a minimum in the summer and maximum in the winter, with the largest monthly differences in sea ice extent occurring in the fall months, peaking in September (Fig. 2.1a). For both simulations, the mid-latitude atmospheric response has been shown to be the most significant in the winter, and as a result, this study focuses on the winter atmospheric response (Vihma, 2014). Figure 2.1b shows the difference in winter sea ice concentration between the EXP and CNTRL. As expected, differences are concentrated in the marginal sea ice zone where sea ice losses can reach 100% (Fig. 2.1b).

2.2 Self-Organizing Maps

To understand the impact of sea ice loss on atmospheric variability, we use a machine learning method called Self-Organizing Maps (SOMs). SOMs can be used to identify and sort large data sets into dominant spatial patterns and calculate the associated frequency of occurrence of each pattern. A benefit of the SOM method is that it does not require patterns to be orthogonal, unlike the more traditional method of empirical orthogonal functions (EOFs). As a result, the SOM method can produce archetypal

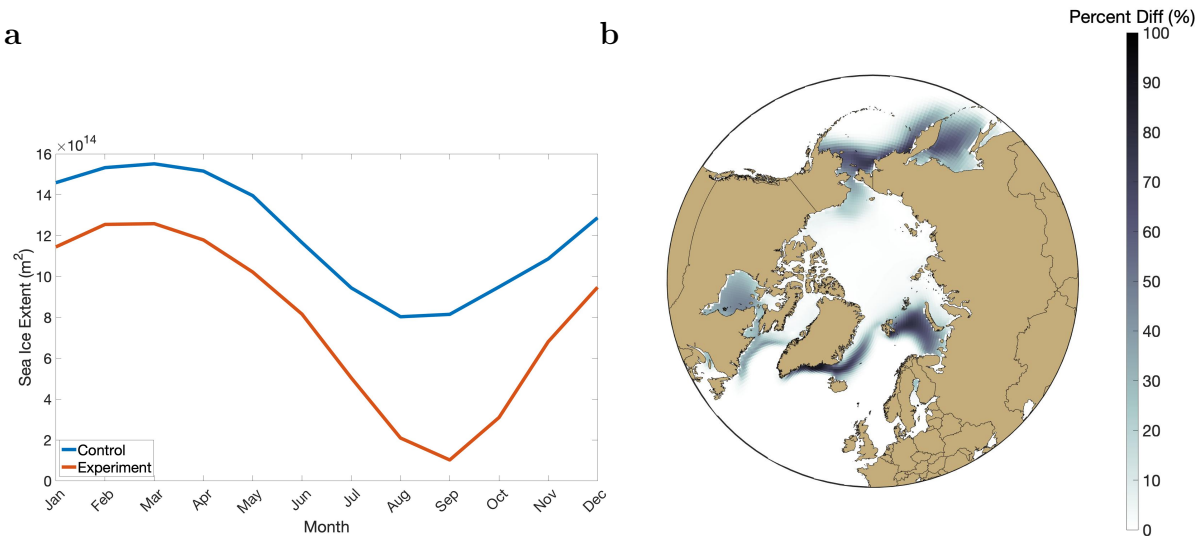

Figure 2.1. a) Seasonal cycle of sea ice extent (m^2) for the CNTRL and EXP, b) Mean difference in winter sea ice concentration (%) between the EXP and CNTRL experiments.

patterns that are more realistic. Unlike K-Means clustering, SOM assumes the data exists on a continuum and organizes the patterns so that more similar patterns are closer together. The SOM algorithm has been used in several atmospheric science studies to characterize synoptic scale circulation patterns (Hewitson and Crane, 2002), investigate future changes in atmospheric variability (Schuenemann and Cassano, 2010; Gervais et al., 2016), predict transitions between sea surface temperature patterns (Gu and Gervais, 2021), and identify differences in jet regimes between model simulations (Gervais et al., 2020).

In this study, we are interested in atmospheric variability over North America in the wintertime, when the impact of sea ice loss on atmospheric circulation is greatest. Our SOM is trained using anomalous 500 hPa geopotential height (Z500) wintertime (December, January, February) data for all 200 years from both the CNTRL and EXP simulations over the region of 25°N to 75°N and 180 °E to 20°E. This region allows us to focus on the North American mid-latitude response to sea ice loss.

The goal of the SOM analysis is to characterize changes in atmospheric variability, and so we are interested in removing the mean impact of sea ice loss from the Z500 data prior to training. It is necessary to remove the daily climatology for each simulation separately, instead of just the seasonal mean, in order to remove the signal of differences in the seasonal cycle between experiments. As seen in Figure 2.2, there are large seasonal mean differences between the CNTRL and EXP simulations. The difference between simulations also varies widely over the course of the year and even within a given season.

For example, the AA signal of positive Z500 differences peaks in January and negative Z500 and sea level pressure (SLP) anomalies associated with the Aleutian Low are strongest in December (Fig. 2.2). Therefore, a daily climatology is computed for each simulation by averaging each calendar day over all years. Anomaly fields are then created by subtracting the daily climatology for the corresponding simulation and calendar day from each day of the simulation. Here the SOM is trained using Z500 anomalies, however the term anomalies will be applied when the same method is used for analysis of additional fields.

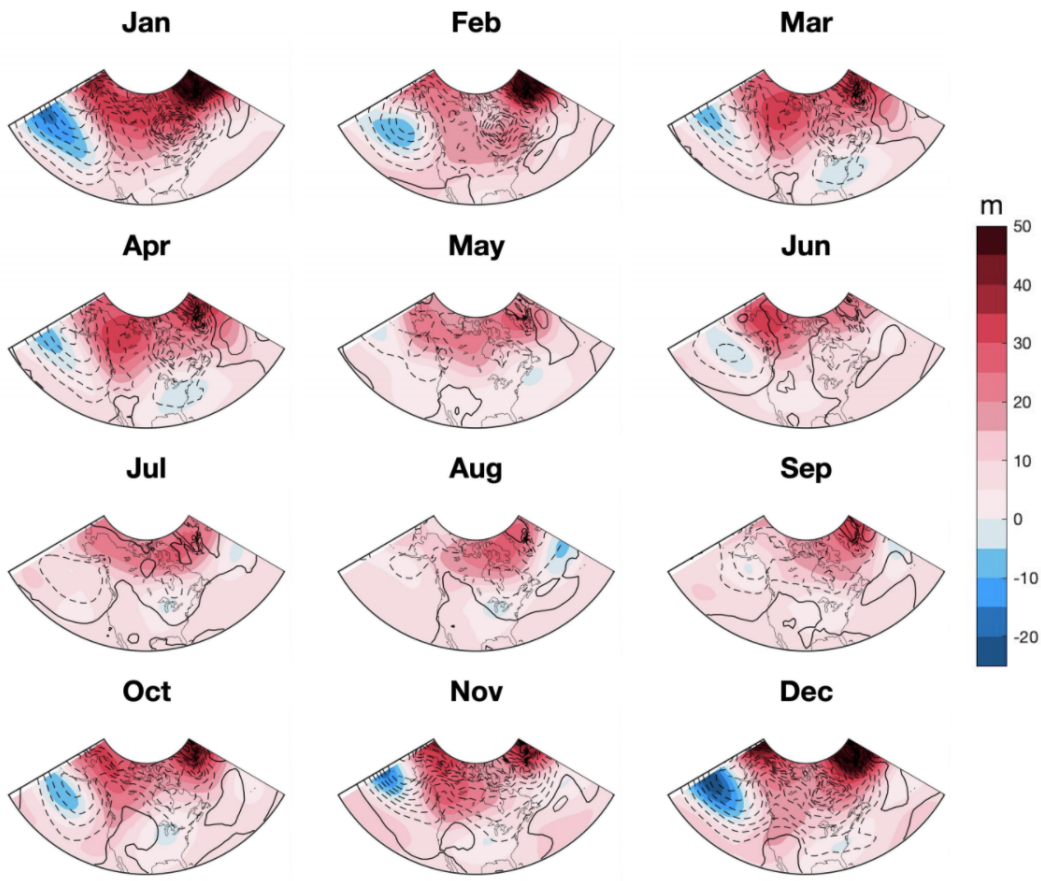

Figure 2.2. Mean monthly differences in Z500 and SLP (Z500 in color, SLP contoured every 5 hPa)

The input data for the SOM consists of these winter Z500 anomalies from both simulations. In training with data from both simulations, we ensure that if a pattern of variability were present in one simulation but not the other, it would still be represented in the SOM. Prior to training, the Z500 anomalies are normalized by removing the mean of the time series and dividing by the standard deviation at each grid point. The data

is then multiplied by the cosine of the latitude so each grid point carries even weight during the computation even though the grid box area changes with latitude.

The number of archetypal patterns or map nodes in the SOM is user determined. After testing different SOM sizes, a 5 x 3 grid of map nodes for a total of 15 nodes captured all the patterns that were physically relevant to the problem without merging patterns. Before the SOM is trained, it is initialized using random data. The training proceeds by repeatedly introducing input data vectors (individual days of Z500 anomalies) to the SOM nodes, and then adjusting the SOM nodes to better match the input data. To accomplish this, the SOM algorithm determines a best matched unit (BMU) for a specific training step (t) by finding the map node (m_i) with the smallest Euclidean distance to the input data vector ($x(t)$). The SOM is then updated using the following relation:

$$m_i(t+1) = m_i(t) + \alpha(t) \cdot h_{ci}(t) \cdot (x(t) - m_i(t)), \tag{2.1}$$

where h(t) is the neighborhood function that defines the relative influence on different map nodes, and $\alpha(t)$ is the learning rate parameter that defines how much the map nodes are updated (Kohonen, 2001; Vesanto et al., 2000). For the neighborhood function we use the Epanechikhov function defined as:

$$h_{ci} = max(0, 1 - \frac{d_{ci}^2}{\sigma(t)^2}), \tag{2.2}$$

where d is the distance between a given node (i) and the BMU (c). For the Epanechikov function, the BMU is modified the most and this decreases with distance away from the BMU. $\sigma(t)$ is the radius of influence and nodes outside of the radius of influence are left unchanged. We use the diameter of the SOM as the initial radius of influence and decrease the value with each training iteration to eventually reach 1. Here we conduct two trainings with different initial $\sigma(t)$. The first training has an initial $\sigma(t)$ of 5 and is important for broad organization. The second training has an initial $\sigma(t)$ of 2 is utilized for fine tuning. For the learning rate parameter we use an inverse function of training time defined as:

$$\alpha(t) = \alpha_0/(1 + 100\frac{t}{L}), \tag{2.3}$$

where α_0 is the initial learning rate for each training. Here we use α_0=0.1 for the first training and α_0=0.01 for the second training.

There are three measures used to assess SOM map quality: topological error, quanti-

zation error, and the Sammon map. Quantization error is the average Euclidean distance between the input data and their associated BMU, thus describing how similar the map nodes are to the input data vectors. The topological error is defined as the percentage of input data vectors for whom the next best match unit is not a neighbor to the BMU and thus quantifies how well-ordered the SOM is. The Sammon map is a nonlinear mapping that visually represents the relative locations of the SOM map nodes. A SOM is well constructed when there is a balance of low quantization error and low topological error (<15 %) and a flat Sammon map. Over-training a SOM can result in a quantization error that continues to decrease at the expense of a twisted Sammon map and higher topological error. The final Sammon Map (Fig. A.1) as well as the quantization error (Fig. A.2) and topological error (Fig. A.3) over the course of each training can be found in the Appendix. More information about the SOM method is available in Kohonen (2001). The SOM Program Package is publicly accessible at http://www.cis.hut.fi/research/som-research/, (Kohonen, 2001).

2.3 SOM Analysis

We use composites (S) to understand the synoptic setup in each node and to provide a better understanding the mechanisms driving each of our SOM patterns. We composite all the days associated with a given node by averaging a given variable across all BMUs for that node. We can do this for all of the input data (S) or only the BMUs associated with either the CNTRL (S_{CNTRL}) or EXP (S_{EXP}) simulation. To characterize difference in pattern in a given node change with sea ice loss, we also compute the difference between the composites (ΔS). This is computed by subtracting S_{CNTRL} from S_{EXP}. ΔS can identify if certain patterns and signals are amplified, de-amplified, or shifted with sea ice loss. Statistical significance at each grid point of ΔS is determined using a student's t-test at a 95% confidence level with a null hypothesis of zero.

The frequency of each pattern can provide insight in how often a node pattern occurs between both experiments or in each simulation separately. This is important because although all patterns are present in both simulations, each pattern becomes more or less frequent with sea ice loss. The frequency of each pattern is computed by totaling the number of BMUs for a given node and dividing by the total number of input days for the entire SOM. The individual frequencies for the CNTRL (f_{CNTRL}) and EXP (f_{EXP}) were computed similarly, but by only using the total number of BMUs and input days for each corresponding simulation. To determine if a frequency difference between simulations was

significant, we utilized a permutation test. BMUs from both simulations are randomly assigned to new "CNTRL" and "EXP" data sets. A new Δf is computed as before and the process is repeated 1000 times in order to create a null distribution of Δf. If the true Δf lies outside the 2.5^{th} or 97.5^{th} percentiles the frequency differences are deemed significant. This process is repeated for each node. (Gervais et al., 2020)

Following Gervais et al. (2020), differences in atmospheric variability between experiments can be defined as arising from differences in frequency of SOM nodes (Δf) or differences in pattern (ΔS). The total difference between simulations for all nodes can be decomposed with the following equation:

$$\Delta(fS) = \sum_{i=1}^{n}(f_{CNTRL,i}S_{CNTRL,i}) + \sum_{i=1}^{n}(f_{EXP,i}S_{EXP,i}) \tag{2.4}$$

where n is the number of SOM nodes, which in the case of our SOM is 15.

This can be further decomposed into a contribution to the total difference due to differences in frequency and pattern as follows:

$$\Delta(fS) = \Delta fS + f\Delta S \tag{2.5}$$

where,

$$\Delta fS = \sum_{i=1}^{n}(f_{EXP,i} - f_{CNTRL,i})\frac{S_{EXP,i} + S_{CNTRL,i}}{2} \tag{2.6}$$

$$f\Delta S = \sum_{i=1}^{n}\frac{f_{EXP,i} + f_{CNTRL,i}}{2}(S_{EXP,i} - S_{CNTRL,i}) \tag{2.7}$$

The input data used in this study has the climatology of each simulation removed separately. As a result, for each simulation the summation over map nodes of frequency times composite mean should be approximately equal to zero. Therefore, the total difference between experiments is also expected to be near zero and so the two terms on the right-hand side of the equation will be roughly equal and opposite.

Chapter 3
Results and Discussion

In our analysis, we look at the mean differences between experiments in section 3.1. We analyze variability between both experiments by computing a SOM of anomalous wintertime Z500 in section 3.2, and we composite additional variables to understand the synoptic setup of each SOM node for the CNTRL. In section 3.3, we look at changes in pattern and frequency of each node between experiments to understand how the nodes change with sea ice loss, and we perform a decomposition of variability to summarize changes across all nodes. We specifically look at the tropospheric changes in variability in section 3.3.1, and the stratospheric response to sea ice loss in section 3.3.2, and the decomposition of variability for specific variables in section 3.3.3.

3.1 Mean Impact of Sea Ice Loss

The winter mean difference between the CNTRL and EXP simulations is shown in Figure 3.1. Here we can see a clear signal of Arctic Amplification with warmer potential temperatures at 850hPa (θ_{850}) that are greatest at the poles and a similar pattern of higher 500hPa geopotential heights consistent with an increase in the mean column temperature (Fig. 3.1a,c). Near regions of sea ice loss (Fig. 2.1) there is a reduction in SLP, which is attributed to the expected thermal low response to sea ice loss (Fig. 3.1b). For example, over the Hudson Bay there are large negative SLP anomalies that reach -5 hPa.

Over the mid-latitudes, the winter mean Z500 and SLP differences show negative anomalies in the North Pacific (Fig. 3.1b,c), which is consistent with a deepened Aleutian low. This is dynamically consistent with the elongation of the Pacific jet as shown in the wind speed on the dynamic tropopause (DT), where the DT is defined as the 2 potential vorticity unit (PVU) surface (Fig. 3.1d). There are also notable changes in the Atlantic

jet on the DT which exhibits an equator-ward shift (Fig. 3.1d), consistent with results from previous studies (Ronalds et al., 2020; Sun et al., 2015; Blackport and Kushner, 2017, 2018; Screen et al., 2018; Deser et al., 2015)

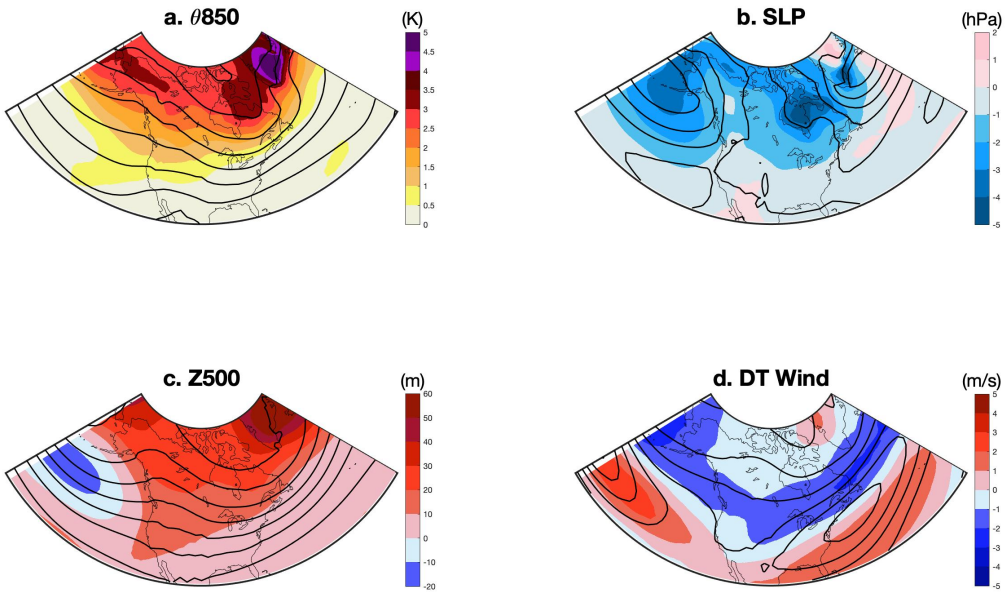

Figure 3.1. Mean winter differences between simulations (EXP - CNTRL) in color and climatology in black contours for a) potential temperature with climatology contoured every 5 K, b) SLP with climatology contoured every 5 hPa, c) Z500 with climatology contoured every 100 m and d) DT wind with climatology contoured every 5 m/s)

3.2 Atmospheric Variability Identified Using SOM

A SOM of daily winter Z500 anomalies can identify dominant synoptic patterns used to understand atmospheric variability over North America (Fig. 3.2). Nodes in the upper left corner have an El Niño-like pattern, and nodes in the bottom right corner have a La Niña-like pattern. Nodes (1,2) and (1,3) are consistent with a negative AO/NAO-like pattern, whereas node (3,2) has a positive AO/NAO-like signal. Although the NAO is an important feature of the northern hemisphere climate variability and exerts an impact on North American weather, our SOM is trained with data over North America and therefore we expect variability over the North Atlantic will have a limited presence as compared to other sources. Nodes (4,1) and (5,1) have a strong positive anomaly over

Alaska that acts to amplify and shift the climatological ridge over the Rockies further east, while node (4,3) has a negative anomaly over Alaska. Nodes (1,1), (1,2), (2,1), and (2,2) exhibit a strengthened Aleutian Low, while nodes (4,3), (5,2), and (5,3) exhibit a weakened Aleutian low. Nodes in the center of the SOM have weaker patterns overall.

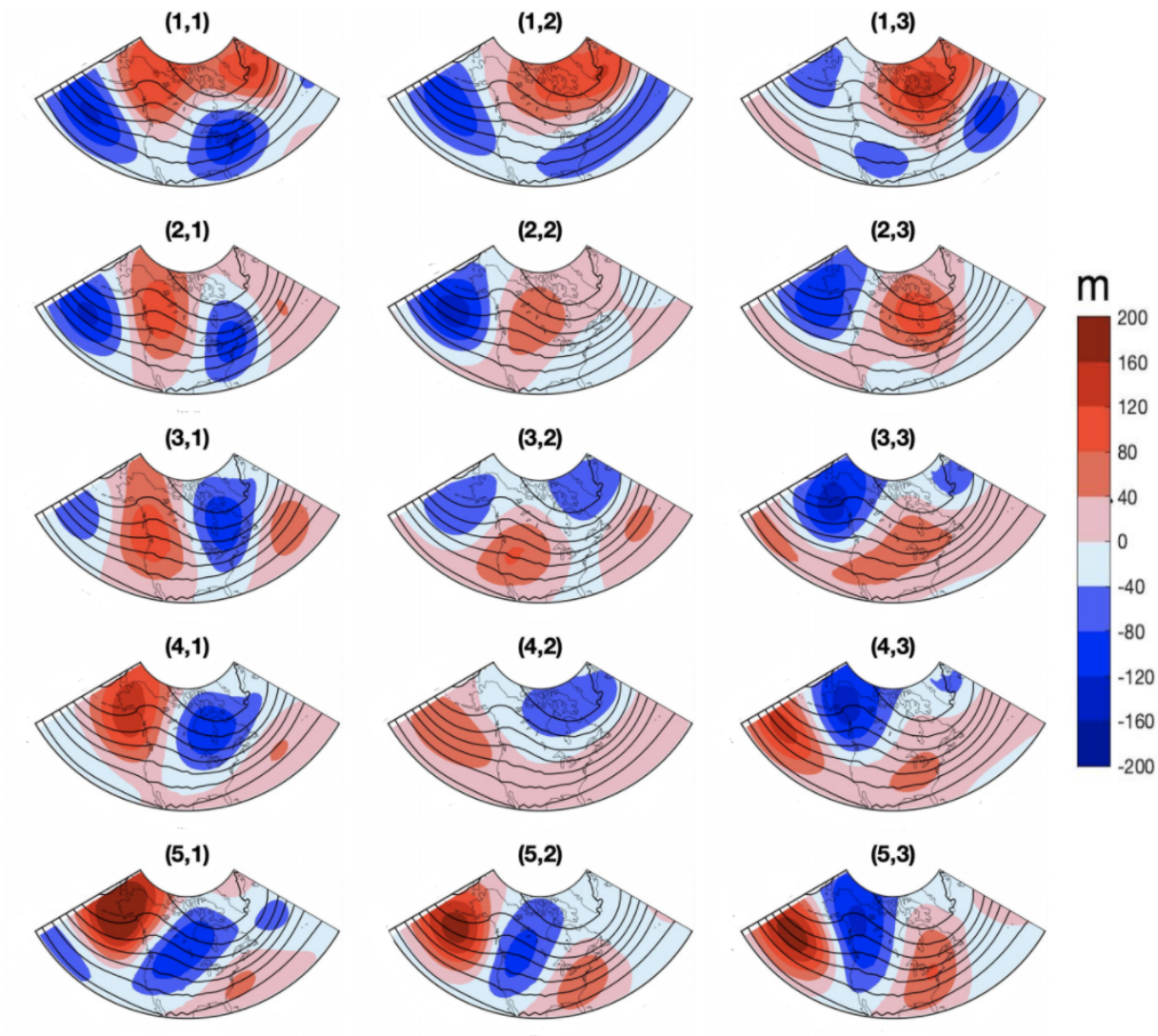

Figure 3.2. SOM of DJF Z500 anomalies (m) over North America in color with the DJF climatological mean Z500 in black contours every 100 m

To obtain further understanding of the synoptic conditions associated with each map node, we compute CNTRL simulation composites (S_{CNTRL}) for additional variables. All variables mentioned are still anomalies with the exception of wind on the DT, which is shown as a full field. Figure 3.3 shows large differences in SLP and θ_{850} from node to

node, but minimal variability in the full field of wind on the DT. Similar to the Z500 anomalies, nodes (1,1), (1,2), (2,1), and (2,2) exhibit a deepened Aleutian Low pattern, while nodes (4,2), (5,2), and (5,3) have positive SLP anomalies over the Pacific. Over the Atlantic there is also evidence of a negative NAO-like SLP anomaly in nodes (1,2) and (1,3) but for many of the remaining nodes the signal in the Atlantic is less coherent.

Although we are not evaluating persistence in this analysis, the θ_{850} patterns in nodes (1,2) and (4,1) are similar to CAOs. Patterns on the left side of the SOM are generally colder, specifically nodes (1,1), (1,2), (3,1), and (4,1). Patterns on the bottom right of the SOM have anomalously warm continental temperatures, specifically nodes (3,3), (4,3), (5,2), and (5,3). The cold nodes are associated with El Nino-like conditions and low pressures over the Pacific, while the warm nodes are associated with La-Nina-like conditions and an elongated Aleutian Low over the Pacific. This elongated Aleutian Low over the Pacific in the warm nodes should act to transport warm, maritime air into the continent. In terms of colder nodes (1,1) and (4,1), both exhibit negative pressures anomalies in the North Atlantic, consistent with characteristics of CAOs found in Smith and Sheridan (2019).

Figure 3.4a,b shows the associated frequency of each map node in the CNTRL and EXP simulations. All node patterns in Figure 3.2 are present in both the CNTRL and EXP simulations. In the CNTRL simulation, nodes (4,3) (3,2), and (4,2) occur most often. These node are all associated with positive θ_{850} anomalies over the continent, and positive SLP anomalies over the Pacific. The nodes that occur least often are (1,1), (1,2), and (2,1), and these nodes all exhibit negative SLP anomalies over the Pacific and cold anomalies over the continent. In the EXP, nodes (2,2), (4,2), and (4,3) occur most often, while nodes (1,1), (2,1), and (3,1) occur least often.

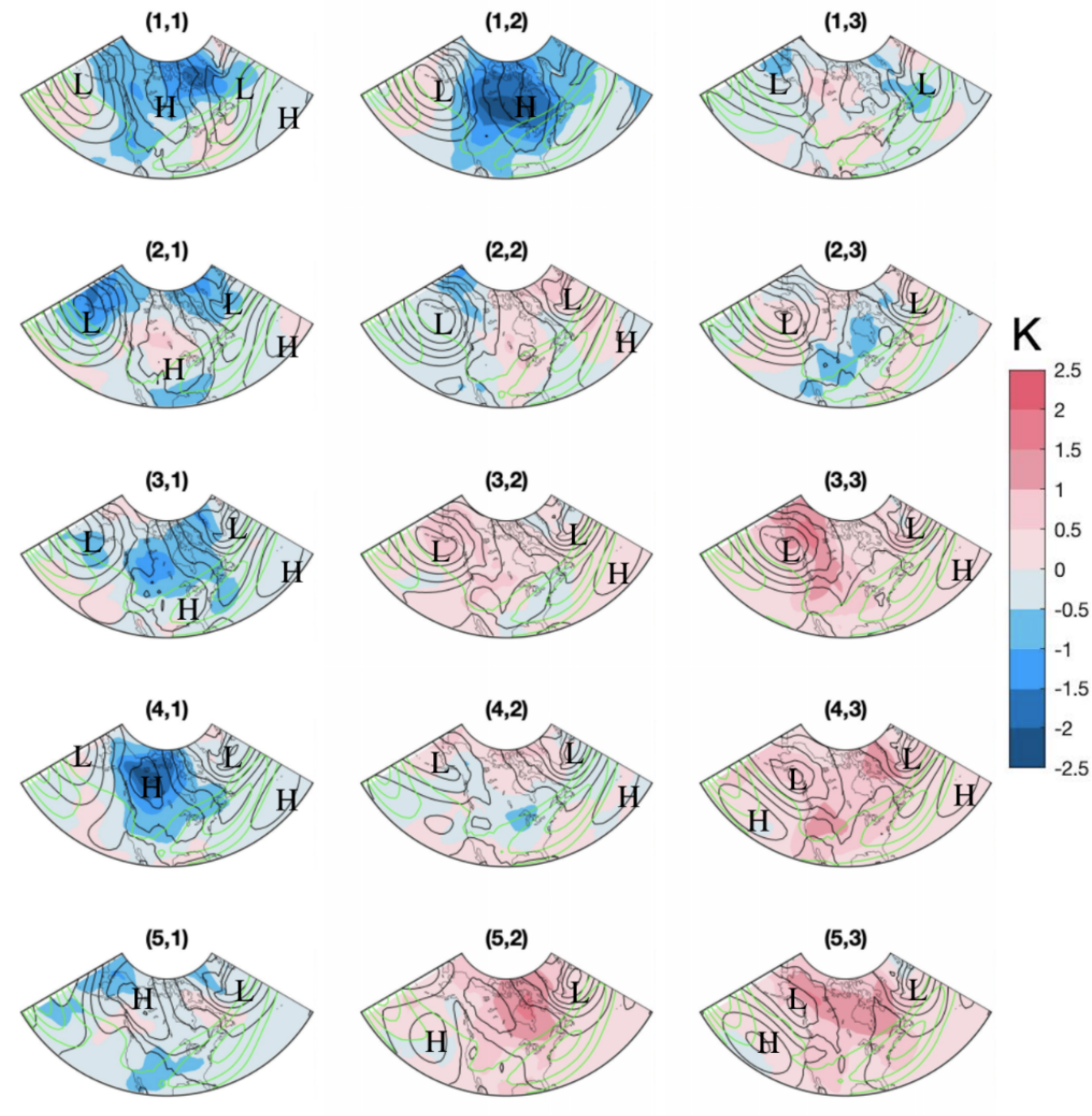

Figure 3.3. CNTRL composites of temperature anomalies (color), SLP anomalies (black contours every 5 mb, positive solid and negative dashed), and DT wind speed (green contours every 5 m/s)

3.3 Impact of Sea Ice Loss on Atmospheric Variability

3.3.1 Tropospheric Response

With the dominant patterns of daily variability in Z500 identified in the SOM analysis, we can further examine how they differ between the CNTRL and EXP simulations. As

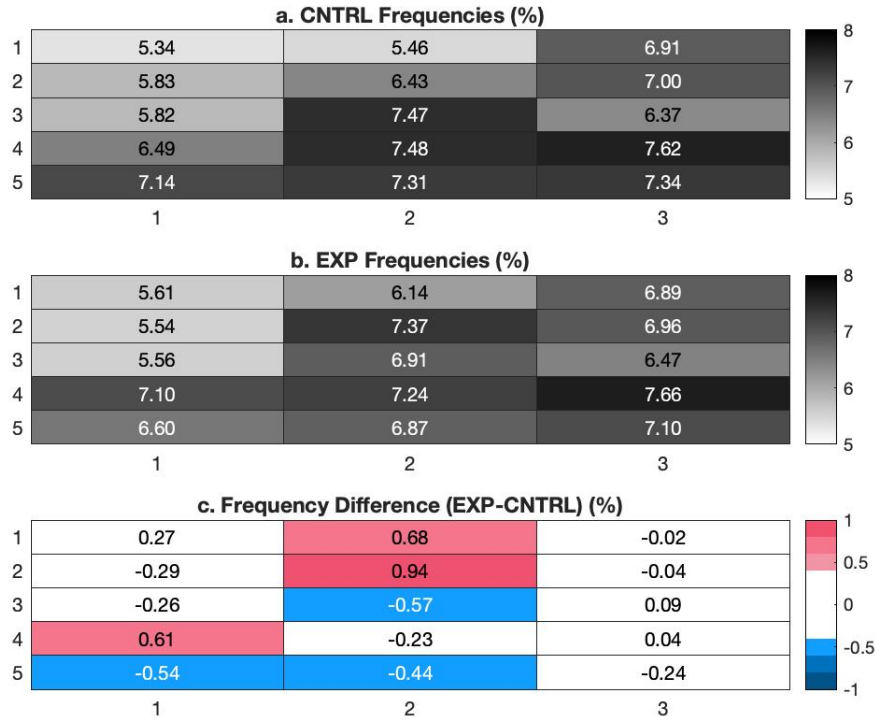

Figure 3.4. Frequency heat map for CNTRL, EXP, and EXP-CNTRL. Significant differences are in color.

described in Gervais et al. (2020), the differences between simulations can be explained through differences in how often the patterns occur, which we define as differences in the frequency of occurrence between the EXP and CNTRL ($\Delta f = f_{EXP} - f_{CNTRL}$). The second is differences in the patterns themselves, which is defined as the composite mean difference between the EXP and CNTRL ($\Delta S = S_{EXP} - S_{CNTRL}$).

Figure 3.4c demonstrates the difference in frequency of each node pattern between the CNTRL and EXP. Node (3,2) decreases in frequency while nodes (1,2) and (2,2) increase in frequency. Because the negative Z500 and SLP anomalies in the Aleutian Low are weaker in node (3,2) than nodes (1,2) and (2,2) (Figs. 3.2 and 3.3), this implies that patterns with deepened Aleutian Lows become more common with sea ice loss. We note that here we have already removed the seasonal mean difference between the experiments that was characterized by a mean deepening of the Aleutian Low and that this result shows further change in how often these deepened Aleutian Low patterns occur. We also see that nodes (5,1) and (5,2) decrease in frequency while node (4,1) increases in frequency with sea ice loss. Since nodes (5,1) and (5,2) have a large positive Z500 over

Alaska and node (4,1) is similar but with a smaller anomaly over Alaska (Fig. 3.2), this can be interpreted as the positive anomaly over Alaska becoming de-amplified. We find that only six nodes show significant changes in frequency, but several more nodes will contribute to changes in variability through significant pattern differences.

For the change in pattern, we can compute the differences in composite mean (ΔS) associated with each SOM node for any variable of interest. We show ΔS for all variables in Figure 3.1 except DT wind whose changes were less coherent and add little to our interpretation (Figs. A.5, A.6). Perhaps the most striking differences lies in the θ_{850} over the continent. In the CNTRL composite for θ_{850} there is a large continental cold anomaly associated with nodes (1,2) and (4,1) (Fig. 3.3). Node (1,2) is also the node with the second largest increase in frequency. For this node, there is a large positive anomaly in ΔS (Fig. 3.5), showing this continental cold anomaly becomes significantly less cold with sea ice loss. Here the positive ΔS anomaly is larger than the cold anomaly of the CNTRL, which shows that this pattern of Z500 is associated with temperature anomalies of opposite signs in the two simulations. Similar, but smaller, amplitude changes can be seen in the adjacent node (1,1). Although we do not include a criteria for persistence typically used to define CAOs, these patterns do resemble a typical CAO in the CNTRL simulation. However, when looking at ΔS, the magnitude of the anomaly associated with the CAO changes sign, indicating that as a result of sea ice loss, these nodes are either becoming less cold (node (4,1)), or actually becoming warmer (node (1,2)) and thus would no longer would be considered a CAO.

Many nodes exhibit smaller but significant negative ΔS anomalies, namely (2,1), (3,1), (2,2), (3,2), (5,2), (3,3), (4,3), and (5,3). These are often associated with warm anomalies in the CNTRL composites, indicating that this relative cooling associated with EXP is associated with a de-amplification of positive anomalies in CNTRL. Several of these patterns, namely (3,3), (4,3), and (5,3), are not associated with significant changes in frequency (Fig. 3.4), so their contribution to changes in variability is solely through a change in pattern.

In summary, these changes in θ_{850} patterns imply that sea ice loss triggers patterns with colder continental temperatures to become less cold, or even warm, but more frequent, and patterns with warmer continental temperatures to become colder relative to the respective simulation's climatology. Although our SOM is computed over North America, it is interesting to note that composites over Europe indicate a connection between CAOs over North America and Europe (Fig. A.4).

Composites of additional circulation variables can provide further understanding of

the mechanisms that produce these differences in θ_{850}. In the ΔS composite differences of SLP (Fig. 3.7) and Z500 (Fig. 3.6), we do not see a clear amplification or de-amplification of the Aleutian Low anomalies discussed previously. Nodes (1,1), (2,1), and (3,1) all exhibit a de-amplification of positive Z500 anomalies over the west coast of the United States (Fig. 3.6). These nodes are accompanied by positive SLP anomalies over the continent (Fig. 3.7), which is de-amplified in nodes (1,1) and (1,2) as seen in the ΔS of SLP. All of these nodes exhibit a localized de-amplification of anomalous ridging over North America. However, changes in θ_{850} appears to be sensitive to the details of these changes are not consistent between nodes.

In nodes in the bottom right corner of the SOM, negative west coast Z500 (Fig. 3.6) and SLP (Fig. 3.7) anomalies are de-amplified (Fig. 3.7). This deamplification can act to reduce the elongation of the Aleutian Low and prevent warmer maritime air from reaching the continent, explaining why the potential temperature differences in Figure 3.5 are negative for nodes (3,3), (4,3), and (5,3). Nodes, (4,1), (5,1), and (5,2) also exhibit shifts in the location of positive SLP and Z500 anomalies in the Pacific. Nodes (1,2) and (1,3) have a deepening of the Icelandic low that acts to reduce the magnitude of the negative NAO signal in these nodes.

3.3.2 Stratospheric Response

Previous studies have found a distinct response of the polar vortex to sea ice loss (Blackport and Kushner, 2017; Nakamura et al., 2016; Sun et al., 2015). In general, the polar vortex acts to isolate air masses in the polar cap allowing them to achieve colder temperatures and prevent polar continental air masses from travelling over the mid-latitude continents. In Figure 3.8, we composite geopotential height at 50 hPa to analyze the stratospheric response to Arctic sea ice loss. In the case of node (1,2), we can see that this pattern is associated with a positive anomaly in Z050 in the CNTRL simulation (Fig. 3.8). This would act to weaken the polar vortex and allow cold polar air to be transported to the continent (Kretschmer et al., 2018). This positive Z050 anomaly in the CNTRL simulation is de-amplified by sea ice loss as seen in the negative Z050 anomalies (Fig. 3.8). However, the de-amplification is insignificant in (1,2), indicating that the increased θ_{850} associated with in this node is not due to circulation changes but purely thermodynamical changes.

Circulation changes in the stratospheric polar vortex are significant and may play a role in creating θ_{850} differences in node (3,2). This node exhibits warm anomalies in over the continent that are de-amplified by the sea ice loss (Fig. 3.5). A low Z050 anomaly

exists over the Arctic in the CNTRL composite that is de-amplified by sea ice loss as seen in the significantly positive ΔS anomalies (Fig. 3.8). This indicates that sea ice loss weakens the polar vortex, which would allow cold polar air to travel towards the continent.

3.3.3 Decomposition of Variability

The total difference in variability across all map nodes can be decomposed into the contribution of change in frequency and in pattern (see Chapter 2, equation 2.5). As discussed in Chapter 2, since the calculations use anomaly data, the contribution of frequency and pattern will be approximately equal and opposite. In our study, there are several instances where a given pattern will increase in frequency but be de-amplified by sea ice loss or vice versa. Decomposing the variability is a useful metric for determining the amalgamated effect of sea ice loss on the region that incorporates all node patterns with their associated frequencies and pattern differences.

Figure 3.9 shows this decomposition for both the geopotential height anomalies at 500 hPa (left) and potential temperature anomalies at 850 hPa (right). From our SOM analysis, we identified several situations where an Aleutian Low pattern becomes more frequent but de-amplified with sea ice loss. The decomposition of variability for Z500 confirms this feature. Figure 3.9 clearly demonstrates a strong Aleutian Low over the Pacific as a result of increased frequency (Fig. 3.9a), but the contribution of change in pattern causes these more frequent deep Aleutian Lows to decrease in magnitude (Fig. 3.9c). Furthermore, while higher Z500 values occur more often in EXP at higher latitudes, they become de-amplified. The southeastern United States exhibits a low Z500 anomaly that increases in frequency and also becomes de-amplified.

The frequency and pattern differences for θ_{850} illustrate that cold air masses become more frequent but warmer, and that warm air masses have insignificant frequency changes, but become colder. When these impacts are summed over all map nodes, the decomposition of potential temperature shows a dipole pattern that splits over Canada and the United States. Ronalds et al. (2020) observed a similar dipole trend, but in their study, cold anomalies over Canada and warm anomalies over the US become more frequent, while in our case, this feature of variability is due to changes in pattern. This could be because Ronalds et al. (2020) clusters based on jet regimes over the North Pacific and does not remove the mean state, whereas our study focuses on Z500 with the mean state removed.

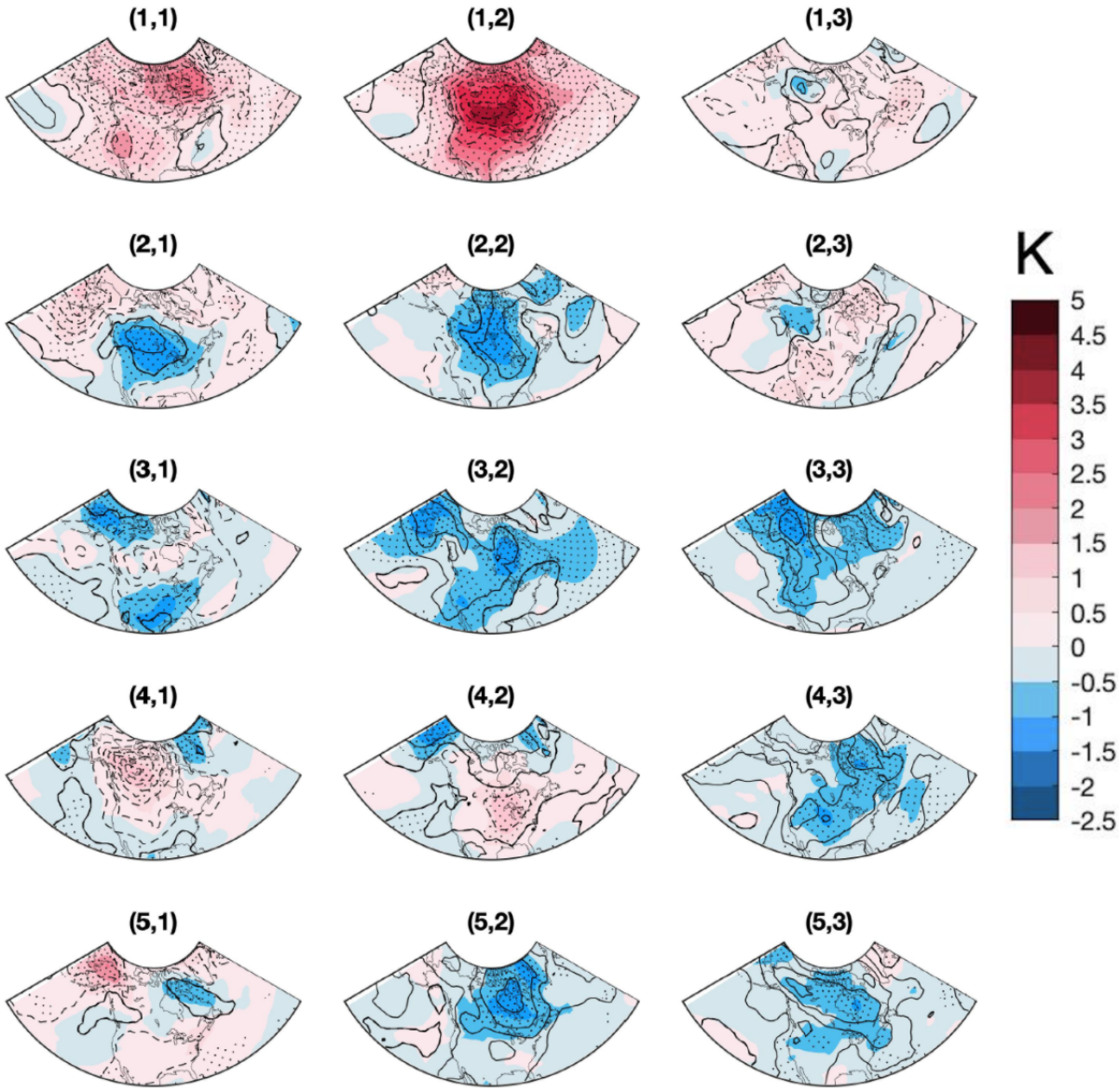

Figure 3.5. θ_{850} anomaly composite; ΔS in color, S_{CNTRL} in contours every 0.25 K provided for reference. Solid contours represent positive anomalies and dashed contours represent negative anomalies.

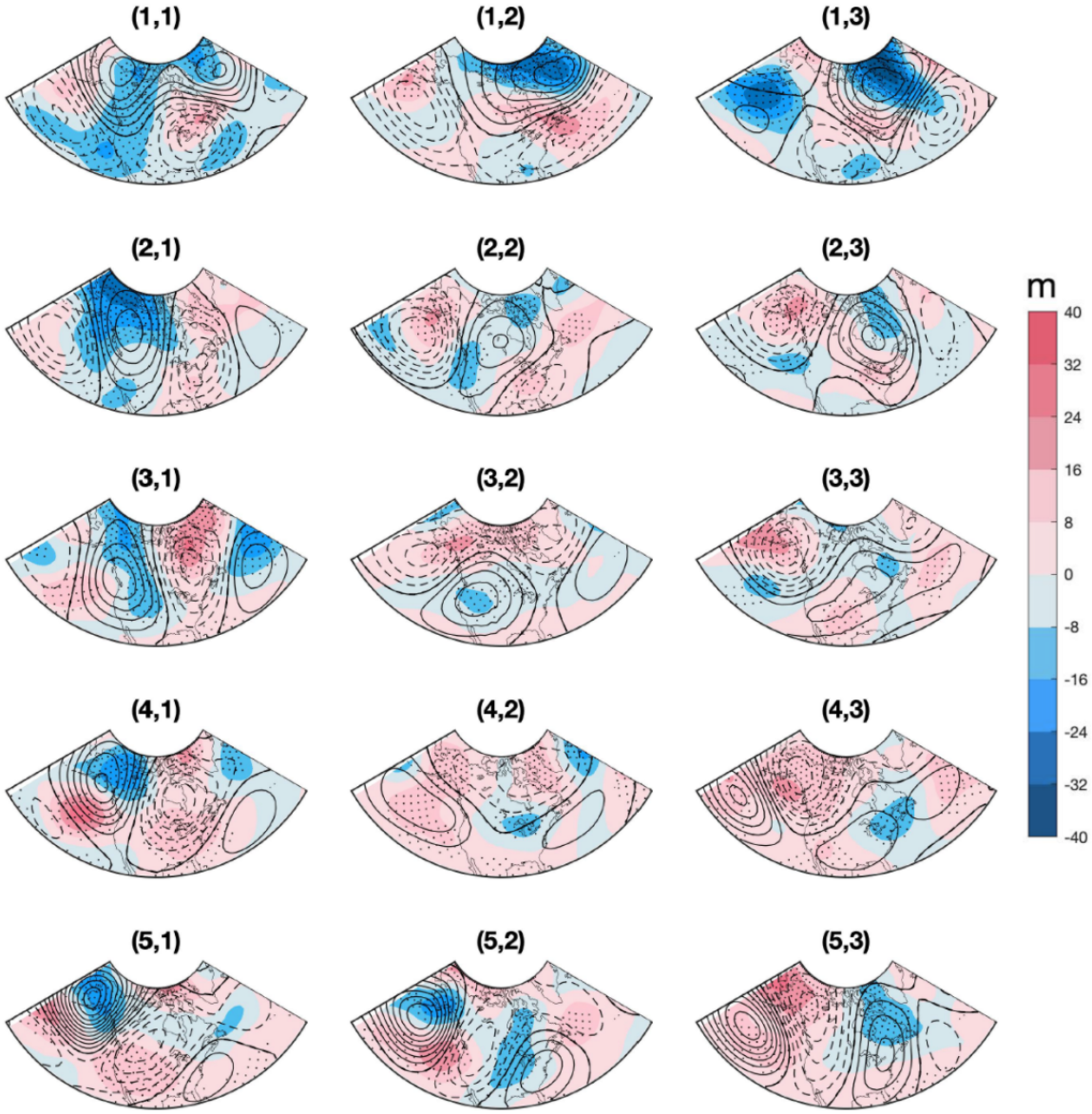

Figure 3.6. Z500 ΔS in color with S_{CNTRL} in contours every 15 m provided for reference. Solid contours represent positive anomalies and dashed contours represent negative anomalies.

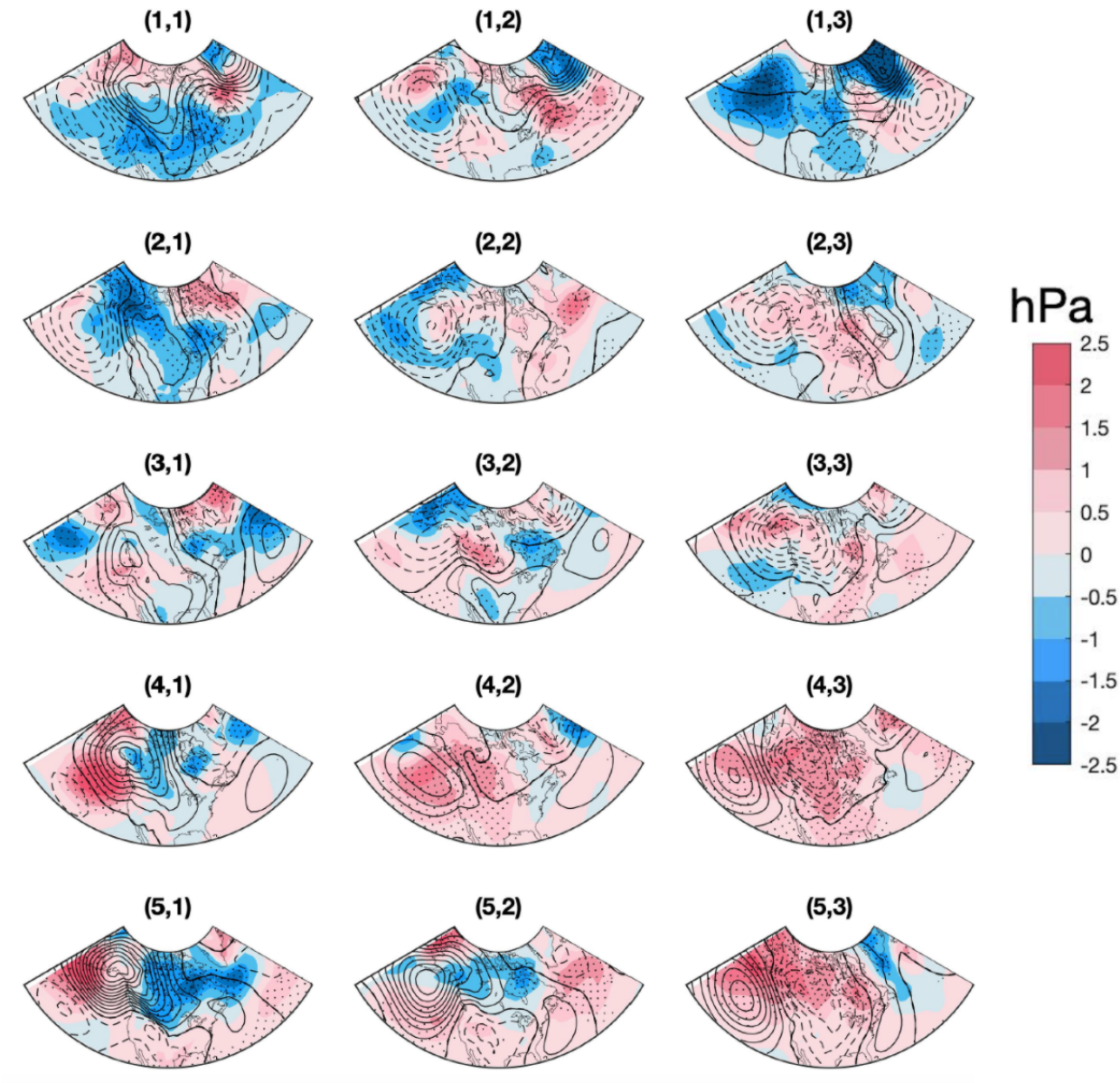

Figure 3.7. SLP ΔS in color with S_{CNTRL} in contours every 2 hPa provided for reference. Solid contours represent positive anomalies and dashed contours represent negative anomalies.

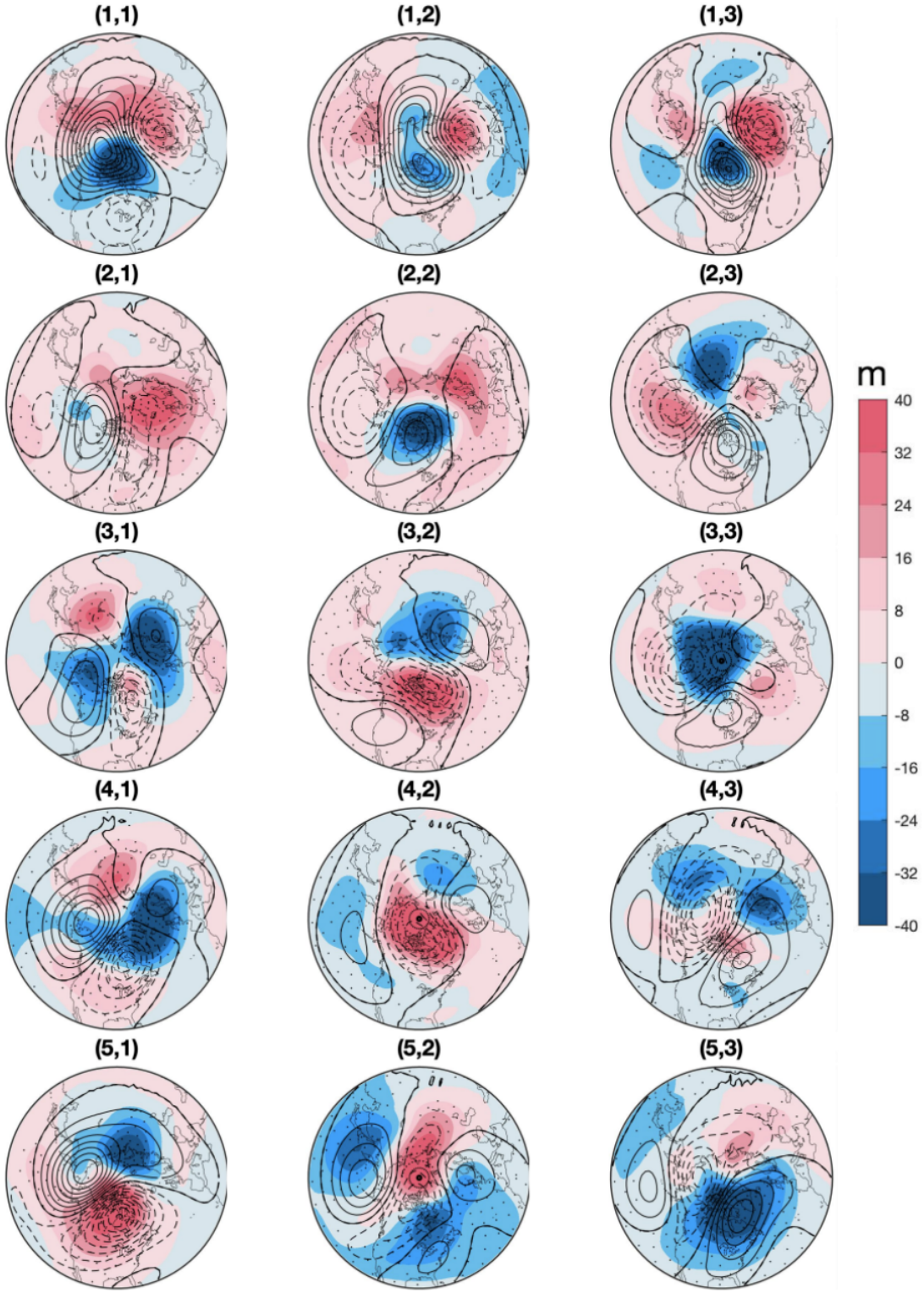

Figure 3.8. Stratospheric analysis of Z050 ΔS in color with S_{CNTRL} in contours every 15 m provided for reference. Solid contours represent positive anomalies and dashed contours represent negative anomalies.

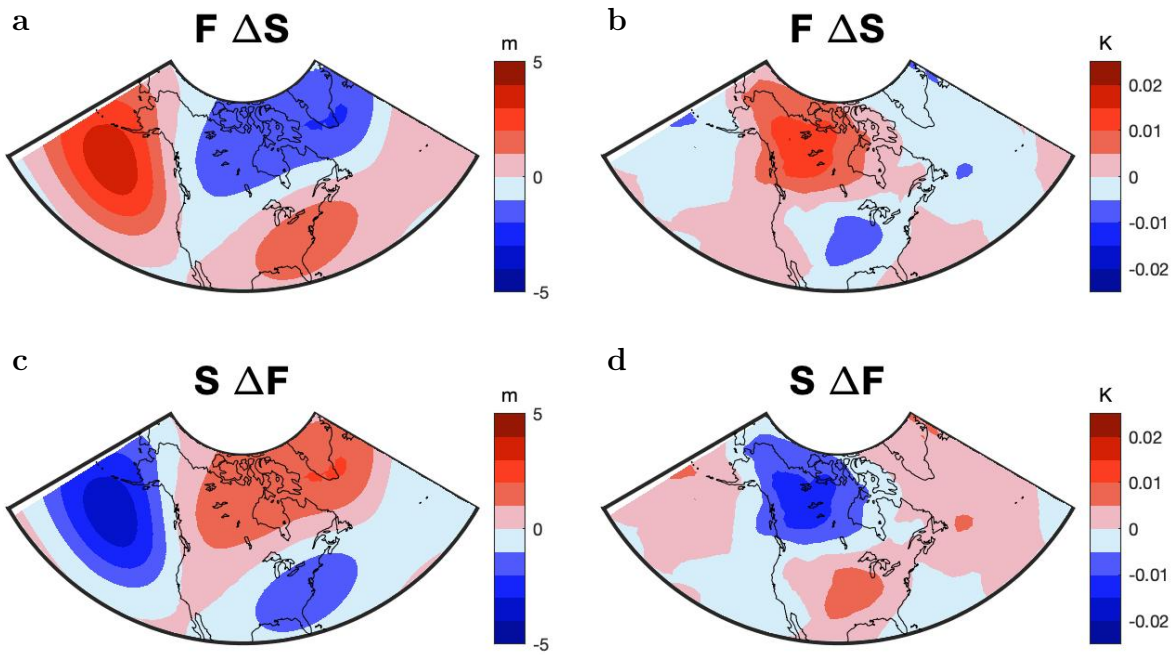

Figure 3.9. Decomposition of SOM variability into contributions from differences in a) and b) patterns and c) and d) frequency for a) and c) Z500 anomalies and b) and d) θ_{850} anomalies

Chapter 4
Conclusion

The goal of this study was to investigate changes in atmospheric variability over North America due to Arctic sea ice loss. We use output from two fully-coupled CESM-WACCM simulations, one with sea ice nudged to the ensemble mean of the WACCM historical runs averaged over 1980-1999, and the other simulation nudged to projected RCP 8.5 values over 2080-2099. A machine learning method, self-organizing maps (SOMs), is used to identify daily weather patterns in anomalous Z500 data that occur in both experiments. We are able to identify changes in variability due to sea ice loss as either changes in node pattern and/or frequency between the two simulations. Although we analyze atmospheric variability through patterns of Z500, we take the difference in composites of other variables between simulations to identify changes in circulation due to sea ice loss and the mechanisms responsible.

We find that patterns with a deepened Aleutian Low become more frequent with sea ice loss and patterns with an intensely amplified Alaskan ridge shift more towards patterns with lesser ridge amplification. These patterns are associated with colder than normal potential temperatures at 850 hPa in the CNTRL simulation. In particular, two of these nodes ((1,2) and (4,1)) have large negative anomalies exceeding 2° and resemble cold air outbreaks (CAOs). These two patterns that resemble CAOs in the CNTRL simulation increase in frequency with sea ice loss but also become less cold, or even warm. Changes in composite of Z500, SLP, and Z050 for these nodes are insignificant, suggesting that changes in circulation are not the primary driver of changes in these patterns. We therefore hypothesize that these associated temperature changes occur primarily through changes in thermodynamics, consistent with Ayarzagüena and Screen (2016).

Nodes with an elongated Aleutian Low over the continent and associated with warm potential temperature anomalies at 850 hPa in the CNTRL do not change in frequency with sea ice loss but do exhibit changes in pattern. In the CNTRL simulation, the

elongated Aleutian Low would act to transport warm maritime air into the continent, explaining the positive temperature anomalies at 850 hPa. With sea ice loss, the Aleutian Low contracts, as seen in significant differences in Z500 and SLP over the North Pacific, resulting in negative temperature differences over the continent. This suggest that these patterns are associated with changes in circulation instead of being dominated by thermodynamic impacts.

With the SOM analysis, the total mean difference between the two experiments can be separated into those caused by changes in the frequency versus changes in the patterns associated with the SOM nodes (Gervais et al., 2020). Given that the mean difference has already been removed, these two impacts will be approximately equal and opposite. The decomposition of Z500 showed a negative change over the Aleutian Low and positive change over Northern Canada and Greenland due to change in frequency, and the opposite due to change in pattern. This indicates that in addition to a mean deepening of the Aleutian Low with sea ice loss, the variability also sees an increase in frequency of days with these deepened Aleutian Low patterns. When the total potential temperature difference was decomposed in this manner, changes in frequency resulted in a dipole pattern over North America with negative anomalies over the northwestern section of the continent and positive anomalies over the southeastern region of the continent. The opposite was found due to changes in node composite pattern.

Our results demonstrate that atmospheric variability is projected to change significantly with Arctic sea ice loss through both changes in frequency of occurrence of a given daily weather pattern and changes in the structure and magnitude of the pattern itself. The use of SOMs to characterize this variability demonstrates the complexity of these changes and the potential for different mechanisms depending on the synoptic pattern. This study raises further questions that warrant investigation including: 1) How does the duration of each pattern vary between simulations? 2) Is there a dynamical connection between changes in cold air outbreaks over North America and over Eurasia? 3) Are these results robust across a range of CMIP class models?

Appendix
Supplemental Figures

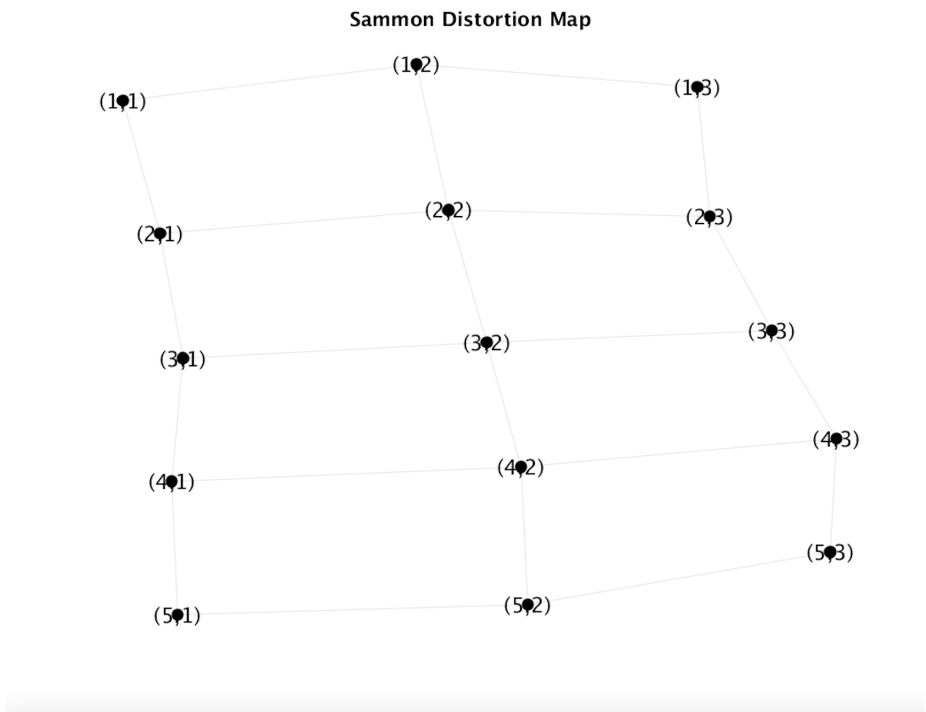

Figure A.1. Sammon map showing the relative Euclidean distances between SOM nodes for the SOM of Z500 anomalies in Figure 3.2

a **b**

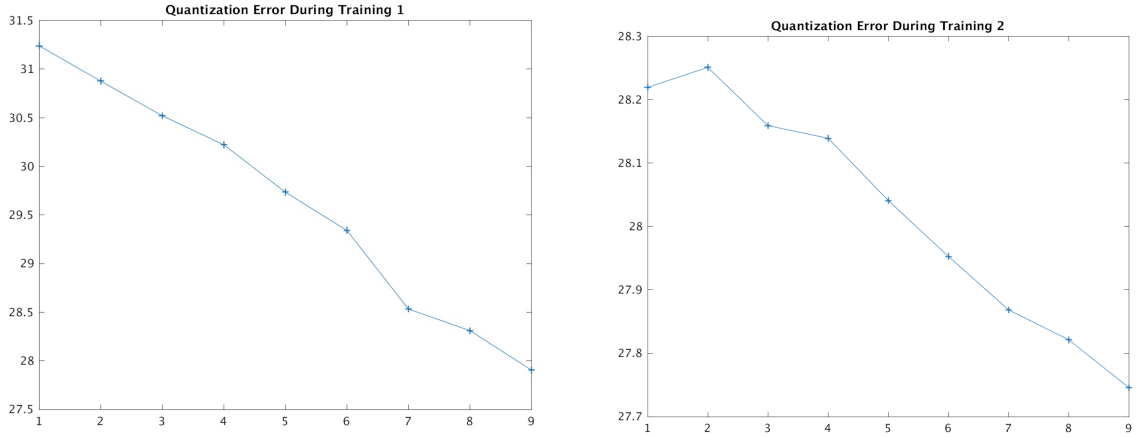

Figure A.2. Quantization Error at several snapshots for a) Training 1, b) Training 2.

a **b**

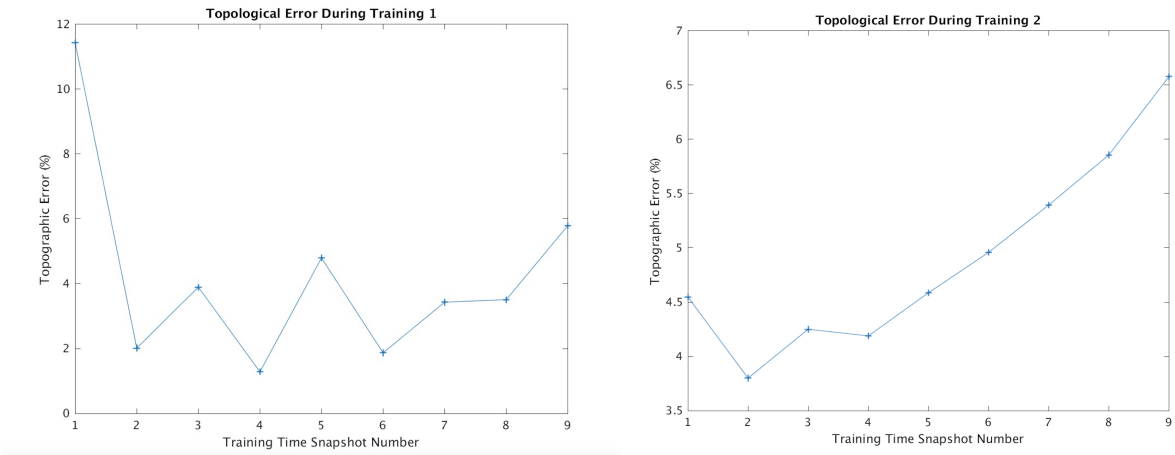

Figure A.3. Topological Error at several snapshots for a) Training 1, b) Training 2.

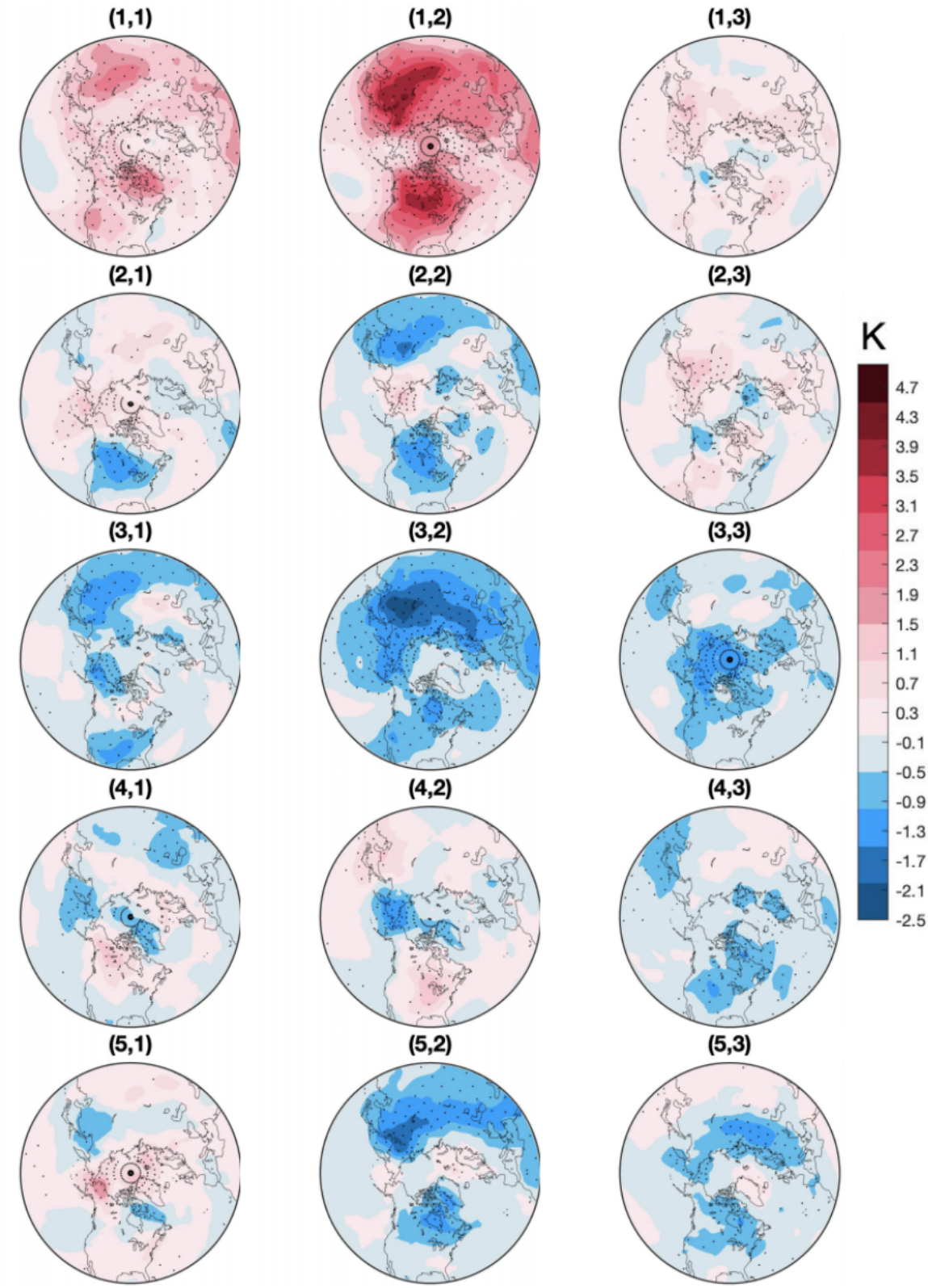

Figure A.4. Polar stereographic view of Θ_{850} ΔS in color

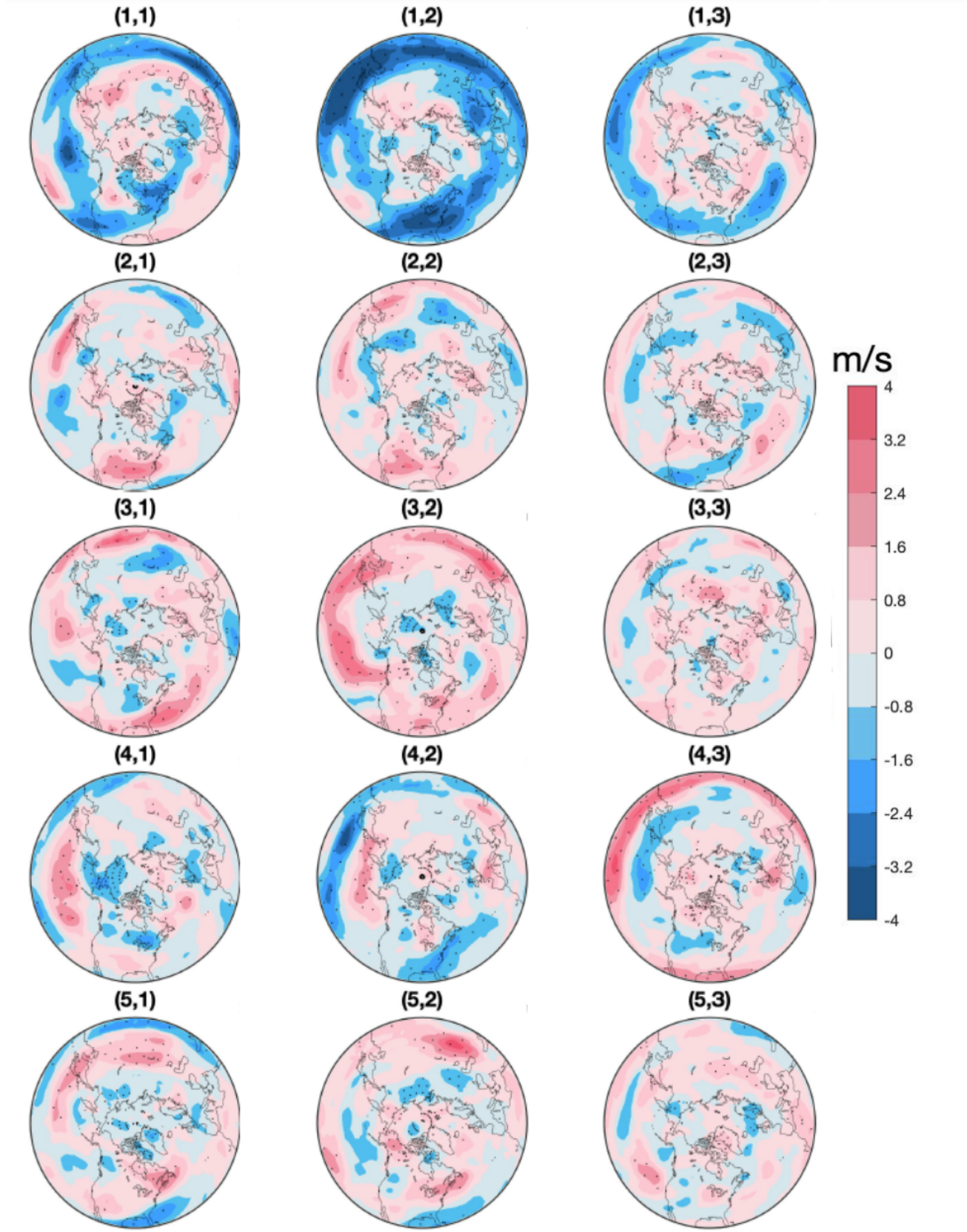

Figure A.5. Polar stereographic view of DT Wind ΔS in color. Result is noisy and was therefore not analyzed further.

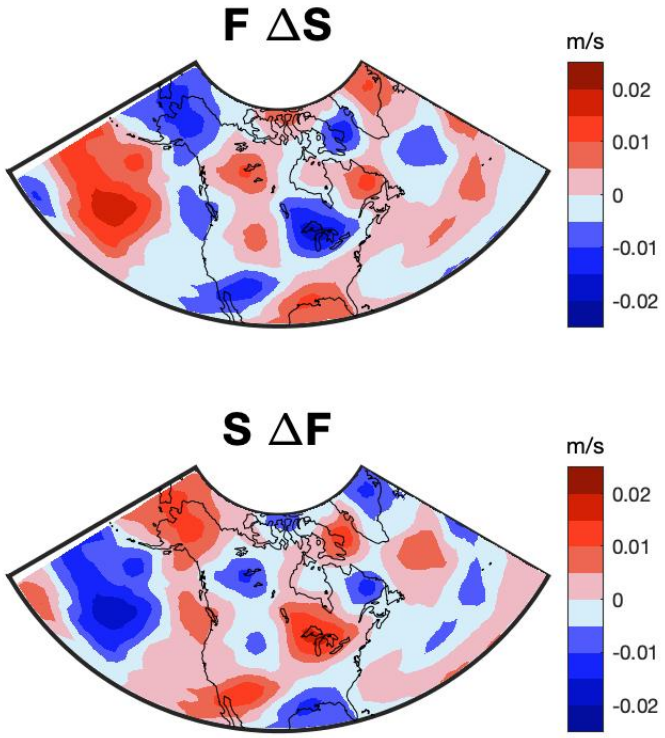

Figure A.6. Decomposition of variability for DT wind. Result is noisy and was therefore not analyzed further.

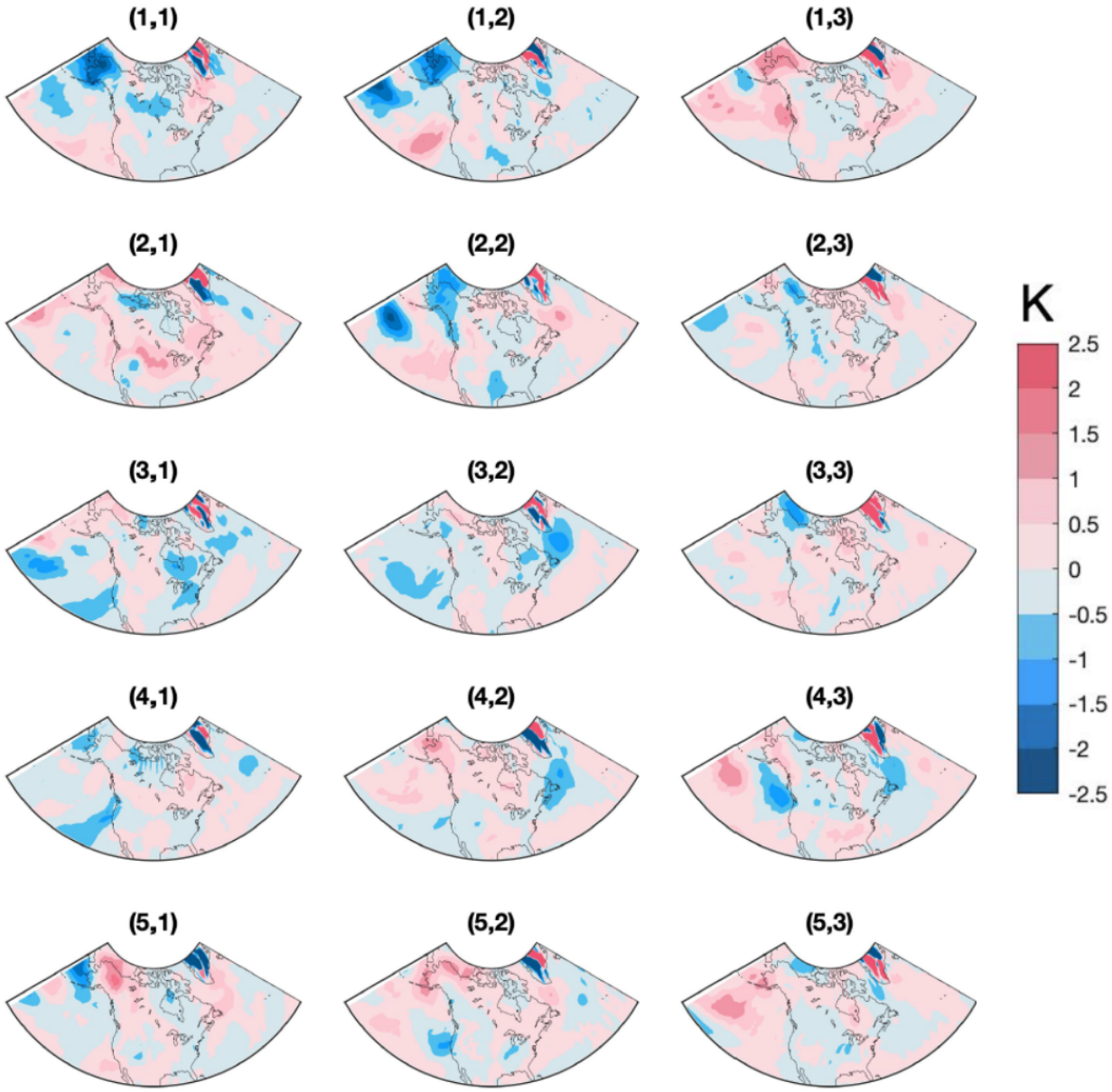

Figure A.7. Polar stereographic view of temperature advection ΔS in color. Result is noisy and was therefore not analyzed further.

Bibliography

Alexander, M. A., U. S. Bhatt, J. E. Walsh, M. S. Timlin, J. S. Miller, and J. D. Scott, 2004: The atmospheric response to realistic arctic sea ice anomalies in an AGCM during winter. *Journal of Climate*, doi:10.1175/1520-0442(2004)017<0890:TARTRA>2.0.CO;2.

Alexeev, V. A., I. Esau, I. V. Polyakov, S. J. Byam, and S. Sorokina, 2012: Vertical structure of recent Arctic warming from observed data and reanalysis products. *Climatic Change*, **111**, 215–239, doi:10.1007/s10584-011-0192-8.

Arrigo, K. R., Z. W. Brown, and M. M. Mills, 2014: Sea ice algal biomass and physiology in the amundsen sea, Antarctica. *Elementa*, **2**, doi:10.12952/journal.elementa.000028.

Ayarzagüena, B., and J. A. Screen, 2016: Future Arctic sea ice loss reduces severity of cold air outbreaks in midlatitudes. *Geophysical Research Letters*, **43 (6)**, 2801–2809, doi:10.1002/2016GL068092.

Barnes, E. A., and L. Polvani, 2013: Response of the midlatitude jets, and of their variability, to increased greenhouse gases in the CMIP5 models. *Journal of Climate*, doi:10.1175/JCLI-D-12-00536.1.

Barnes, E. A., and J. A. Screen, 2015: The impact of Arctic warming on the midlatitude jet-stream: Can it? has it? will it? *Wiley Interdisciplinary Reviews: Climate Change*, doi:10.1002/wcc.337.

Blackport, R., and P. J. Kushner, 2017: Isolating the atmospheric circulation response to Arctic sea ice loss in the coupled climate system. *Journal of Climate*, doi:10.1175/JCLI-D-16-0257.1.

Blackport, R., and P. J. Kushner, 2018: The role of extratropical ocean warming in the coupled climate response to arctic sea ice loss. *Journal of Climate*, doi:10.1175/JCLI-D-18-0192.1.

Chen, X., and D. Luo, 2017: Arctic sea ice decline and continental cold anomalies: Upstream and downstream effects of greenland blocking. *Geophysical Research Letters*, **44**, 3411–3419, doi:10.1002/2016GL072387.

Cohen, J., and Coauthors, 2014: Recent Arctic amplification and extreme mid-latitude weather. Nature Publishing Group, 627-637 pp., doi:10.1038/ngeo2234.

Dai, A., and J. Deng, 2021: Arctic amplification weakens the variability of daily temperatures over northern middle-high latitudes. *Journal of Climate*, **34**, doi: 10.1175/JCLI-D-20-0514.1.

Deser, C., G. Magnusdottir, R. Saravanan, and A. Phillips, 2004: The effects of North Atlantic SST and sea ice anomalies on the winter circulation in CCM3. Part II: Direct and indirect components of the response. *Journal of Climate*, doi:10.1175/1520-0442(2004)017<0877:TEONAS>2.0.CO;2.

Deser, C., R. A. Tomas, and L. Sun, 2015: The role of ocean-atmosphere coupling in the zonal-mean atmospheric response to Arctic sea ice loss. *Journal of Climate*, **28**, 2168–2186, doi:10.1175/JCLI-D-14-00325.1.

Francis, J. A., and S. J. Vavrus, 2012: Evidence linking Arctic amplification to extreme weather in mid-latitudes. *Geophysical Research Letters*.

Gervais, M., E. Atallah, J. R. Gyakum, and L. B. Tremblay, 2016: Arctic air masses in a warming world. *Journal of Climate*, **29**, doi:10.1175/JCLI-D-15-0499.1.

Gervais, M., J. Shaman, and Y. Kushnir, 2020: Impact of the North Atlantic warming hole on sensible weather. *Journal of Climate*, **33**, 4255–4271, doi:10.1175/JCLI-D-19-0636.1.

Gu, Q., and M. Gervais, 2021: Exploring North Atlantic and North Pacific decadal climate prediction using self-organizing maps. *Journal of Climate*, **34**, doi:10.1175/JCLI-D-20-0017.1.

Hewitson, B., and R. Crane, 2002: Self-organizing maps: applications to synoptic climatology. *Climate Research*, **22**, doi:10.3354/cr022013.

Holland, M. M., and C. M. Bitz, 2003: Polar amplification of climate change in coupled models. *Climate Dynamics*, **21**, 221–232, doi:10.1007/s00382-003-0332-6.

Honda, M., J. Inoue, and S. Yamane, 2009: Influence of low Arctic sea-ice minima on anomalously cold Eurasian winters. *Geophysical Research Letters*, **36**, doi:10.1029/2008GL037079.

Hopsch, S., J. Cohen, and K. Dethloff, 2012: Analysis of a link between fall Arctic sea ice concentration and atmospheric patterns in the following winter. *Tellus A: Dynamic Meteorology and Oceanography*, **64**, doi:10.3402/tellusa.v64i0.18624.

Hunke, E. C., W. H. Lipscomb, A. K. Turner, N. Jeffery, and S. Elliott, 2015: CICE: the Los Alamos Sea Ice model documentation and software user's manual version 5.1 la-cc-06-012. URL http://oceans11.lanl.gov/trac/CICE/wiki.

Hurrell, J. W., and Coauthors, 2013: The community earth system model: A framework for collaborative research. *Bulletin of the American Meteorological Society*, **94**, 1339–1360, doi:10.1175/BAMS-D-12-00121.1.

Inoue, J., M. E. Hori, and K. Takaya, 2012: The role of Barents sea ice in the wintertime cyclone track and emergence of a warm-Arctic cold-Siberian anomaly. *Journal of Climate*, **25**, doi:10.1175/JCLI-D-11-00449.1.

Jahn, A., 2018: Reduced probability of ice-free summers for 1.5 °c compared to 2 °c warming. *Nature Climate Change*, doi:10.1038/s41558-018-0127-8.

Jaiser, R., K. Dethloff, and D. Handorf, 2013: Stratospheric response to Arctic sea ice retreat and associated planetary wave propagation changes. *Tellus A: Dynamic Meteorology and Oceanography*, **65**, doi:10.3402/tellusa.v65i0.19375.

Kohonen, T., 2001: *Self-Organzing Maps*.

Kretschmer, M., D. Coumou, L. Agel, M. Barlow, E. Tziperman, and J. Cohen, 2018: More-persistent weak stratospheric polar vortex states linked to cold extremes. *Bulletin of the American Meteorological Society*, **99**, doi:10.1175/BAMS-D-16-0259.1.

Kumar, A., and Coauthors, 2010: Contribution of sea ice loss to Arctic amplification. *Geophysical Research Letters*, **37**, doi:10.1029/2010GL045022.

Magnusdottir, G., C. Deser, and R. Saravanan, 2004: The effects of North Atlantic SST and sea ice anomalies on the winter circulation in CCM3. part I: Main features and storm track characteristics of the response. *Journal of Climate*, doi:10.1175/1520-0442(2004)017<0857:TEONAS>2.0.CO;2.

Matsuno, T., 1971: A dynamical model of the stratospheric sudden warming. *Journal of the Atmospheric Sciences*, **28**, doi:10.1175/1520-0469(1971)028<1479:ADMOTS>2.0.CO;2.

Meleshko, V. P., O. M. Johannessen, A. V. Baidin, T. V. Pavlova, and V. A. Govorkova, 2016: Arctic amplification: does it impact the polar jet stream? *Tellus A: Dynamic Meteorology and Oceanography*, **68**, doi:10.3402/tellusa.v68.32330.

Mori, M., M. Watanabe, H. Shiogama, J. Inoue, and M. Kimoto, 2014: Robust Arctic sea-ice influence on the frequent Eurasian cold winters in past decades. *Nature Geoscience*, **7**, 869–873, doi:10.1038/ngeo2277.

Nakamura, T., K. Yamazaki, K. Iwamoto, M. Honda, Y. Miyoshi, Y. Ogawa, Y. Tomikawa, and J. Ukita, 2016: The stratospheric pathway for Arctic impacts on midlatitude climate. *Geophysical Research Letters*, **43**, 3494–3501, doi:10.1002/2016GL068330.

Nakamura, T., K. Yamazaki, K. Iwamoto, M. Honda, Y. Miyoshi, Y. Ogawa, and J. Ukita, 2015: A negative phase shift of the winter AO/NAO due to the recent arctic sea-ice reduction in late autumn. *Journal of Geophysical Research: Atmospheres*, **120**, doi:10.1002/2014JD022848.

Oudar, T., E. Sanchez-Gomez, F. Chauvin, J. Cattiaux, L. Terray, and C. Cassou, 2017: Respective roles of direct GHG radiative forcing and induced Arctic sea ice loss on the northern hemisphere atmospheric circulation. *Climate Dynamics*, **49**, doi:10.1007/s00382-017-3541-0.

Overland, J. E., K. R. Wood, and M. Wang, 2011: Warm arctic—cold continents: climate impacts of the newly open arctic sea. *Polar Research*, **30**, doi:10.3402/polar.v30i0.15787.

Pedersen, R. A., I. Cvijanovic, P. L. Langen, and B. M. Vinther, 2016: The impact of regional arctic sea ice loss on atmospheric circulation and the nao. *Journal of Climate*, **29**, doi:10.1175/JCLI-D-15-0315.1.

Perovich, D. K., and C. Polashenski, 2012: Albedo evolution of seasonal arctic sea ice. *Geophysical Research Letters*, **39**, doi:10.1029/2012GL051432.

Pithan, F., and T. Mauritsen, 2014: Arctic amplification dominated by temperature feedbacks in contemporary climate models. *Nature Geoscience*, **7**, doi:10.1038/ngeo2071.

Rinke, A., K. Dethloff, W. Dorn, D. Handorf, and J. C. Moore, 2013: Simulated Arctic atmospheric feedbacks associated with late summer sea ice anomalies. *Journal of Geophysical Research: Atmospheres*, **118**, doi:10.1002/jgrd.50584.

Ronalds, B., E. A. Barnes, R. Eade, Y. Peings, and M. Sigmond, 2020: North Pacific zonal wind response to sea ice loss in the Polar Amplification Model Intercomparison Project and its downstream implications. *Climate Dynamics*, **55**, 1779–1792, doi:10.1007/s00382-020-05352-w, URL https://doi.org/10.1007/s00382-020-05352-w.

Schuenemann, K. C., and J. J. Cassano, 2010: Changes in synoptic weather patterns and Greenland precipitation in the 20th and 21st centuries: 2. analysis of 21st century atmospheric changes using self-organizing maps. *Journal of Geophysical Research*, **115**, doi:10.1029/2009JD011706.

Screen, J. A., 2014: Arctic amplification decreases temperature variance in northern mid- to high-latitudes. *Nature Climate Change*, **4**, doi:10.1038/nclimate2268.

Screen, J. A., 2017: Simulated atmospheric response to regional and pan-arctic sea ice loss. *Journal of Climate*, doi:10.1175/JCLI-D-16-0197.1.

Screen, J. A., and I. Simmonds, 2010: Increasing fall-winter energy loss from the Arctic ocean and its role in Arctic temperature amplification. *Geophysical Research Letters*, **37**, doi:10.1029/2010GL044136.

Screen, J. A., and Coauthors, 2018: Consistency and discrepancy in the atmospheric response to Arctic sea-ice loss across climate models. *Nature Geoscience*, doi:10.1038/s41561-018-0059-y.

Serreze, M. C., A. P. Barrett, J. C. Stroeve, D. N. Kindig, and M. M. Holland, 2009: The emergence of surface-based Arctic amplification. URL www.the-cryosphere.net/3/11/2009/, 11-19 pp.

Serreze, M. C., and J. A. Francis, 2006: The arctic amplification debate. *Climatic Change*, **76**, 241–264, doi:10.1007/s10584-005-9017-y.

Serreze, M. C., and Coauthors, 2000: Observational evidence of recent change in the northern high-latitude environment.

Smith, D. M., and Coauthors, 2019: The Polar Amplification Model Intercomparison Project (PAMIP) contribution to CMIP6: investigating the causes and consequences of polar amplification. *Geoscientific Model Development*, **12**, doi:10.5194/gmd-12-1139-2019.

Smith, E. T., and S. C. Sheridan, 2019: The influence of atmospheric circulation patterns on cold air outbreaks in the eastern united states. *International Journal of Climatology*, **39**, doi:10.1002/joc.5935.

Stroeve, J. C., V. Kattsov, A. Barrett, M. Serreze, T. Pavlova, M. Holland, and W. N. Meier, 2012: Trends in arctic sea ice extent from cmip5, cmip3 and observations. *Geophysical Research Letters*, **39**, doi:10.1029/2012GL052676.

Sun, L., C. Deser, and R. A. Tomas, 2015: Mechanisms of stratospheric and tropospheric circulation response to projected arctic sea ice loss. *Journal of Climate*, **28**, 7824–7845, doi:10.1175/JCLI-D-15-0169.1.

Sun, L., J. Perlwitz, and M. Hoerling, 2016: What caused the recent "warm Arctic, cold continents" trend pattern in winter temperatures? *Geophysical Research Letters*, **43**, 5345–5352, doi:10.1002/2016GL069024.

Vavrus, S., J. E. Walsh, W. L. Chapman, and D. Portis, 2006: The behavior of extreme cold air outbreaks under greenhouse warming. *International Journal of Climatology*, **26**, doi:10.1002/joc.1301.

Vesanto, J., J. Himberg, E. Alhoniemi, and J. Parhankangas, 2000: *SOM Toolbox for Matlab 5 Juha Vesanto , Johan Himberg , SOM Toolbox Team Helsinki University of Technology Report A57 April 2000 ISBN 951-22-4951-0 ISSN 1456-2243 Libella Oy Espoo 2000 SOM Toolbox for Matlab 5.* 0-59 pp.

Vihma, T., 2014: Effects of arctic sea ice decline on weather and climate: A review. *Surveys in Geophysics*, **35**, 1175–1214, doi:10.1007/s10712-014-9284-0.

Walsh, J. E., a. S. Phillips, D. H. Portis, and W. L. Chapman, 2001: Extreme cold outbreaks in the united states and europe, 1948-99. *Journal of Climate*, **14**, 2642–2658, doi:10.1175/1520-0442(2001)014<2642:ECOITU>2.0.CO;2.

Wang, M., and J. E. Overland, 2012: A sea ice free summer arctic within 30 years: An update from cmip5 models. *Geophysical Research Letters*, **39**, 6–11, doi:10.1029/2012GL052868.

Williams, M. Z., M. Gervais, and C. E. Forest, 2021: Causes and impacts of sea ice variability in the sea of okhotsk using cesm-le. *Climate Dynamics*, **56**, 2007–2021, doi:10.1007/s00382-020-05572-0.